www.MaterialsViews.com

ADVANCED
OPTICAL
MATERIALS
www.advopticalmat.de

REVIEW

Heterogeneously Integrated Optoelectronic Devices Enabled by Micro-Transfer Printing

Jongseung Yoon,* Sung-Min Lee, Dongseok Kang, Matthew A. Meitl, Christopher A. Bower, and John. A. Rogers*

Transfer printing is a materials assembly technique that uses elastomeric stamps for heterogeneous integration of various classes of micro- and nano-structured materials into two- and three-dimensionally organized layouts on virtually any type of substrate. Work over the past decade demonstrates that the capabilities of this approach create opportunities for a wide range of device platforms, including component- and system-level embodiments in unusual optoelectronic technologies with characteristics that cannot be replicated easily using conventional manufacturing or growth techniques. This review presents recent progress in functional materials and advanced transfer printing methods, with a focus on active components that emit, absorb, and/or transport light, ranging from solar cells to light-emitting diodes, lasers, photodetectors, and integrated collections of these in functional systems, where the key ideas provide unique solutions that address limitations in performance and/or functionality associated with traditional technologies. High-concentration photovoltaic modules based on multijunction, micro- and millimeter-scale solar cells and high-resolution emissive displays based on microscale inorganic light-emitting diodes provide examples of some of the most sophisticated systems, geared toward commercialization.

1. Introduction

Many advances in science and technology follow from capabilities for combining dissimilar materials in unconventional formats. The resulting heterogeneously integrated systems will feature prominently in future technological developments, where cost-competitive, scalable strategies allow integration of diverse materials with complementary performance attributes in ways that do not limit their intrinsic properties.[1–5] Transfer printing, an emerging, high-speed method for materials assembly, provides unique features in this context; it represents an enabling manufacturing technique that offers a simple yet remarkably versatile scheme for manipulating material elements with dimensions ranging from nanometers to centimeters and arranging them into functional devices and systems.[6–8] Here, a soft stamp serves as a tool for removing such elements from a source substrate and delivering them to a target surface, in a massively parallel fashion under ambient conditions, thereby allowing the co-integration of dissimilar materials: single-crystalline materials with various lattice constants and noncrystalline materials; those with high and low thermal stability; those with high and low moduli, and so on. Many of the most prominent examples involve transfer printing with semiconducting, device-grade, inorganic materials such as silicon nanomembranes or III–V platelets to form 2D and 3D assemblies on foreign substrates such as plastic foils or rubber slabs in flexible and stretchable electronics. The results provide high-performance characteristics from materials optimized for their respective roles, independent of concerns of epitaxy, growth conditions, thermal budgets, solvent compatibility, or others.

This review highlights recent advances in heterogeneously integrated optoelectronic devices enabled by transfer printing, ranging from solar cells to light-emitting diodes (LEDs), lasers, photodetectors, and digital imaging systems. Detailed descriptions of methods of transfer printing and their application in other technologies can be found elsewhere.[6,7,9,10] In all cases, transfer printing bypasses many key challenges in traditional processing and fabrication approaches, thereby creating new functionalities and/or enhancing the performance and cost-effectiveness of existing ones. Emerging commercial

Prof. J. Yoon, Dr. S.-M. Lee, D. Kang
Mork Family Department of Chemical Engineering
and Materials Science
University of Southern California
Los Angeles, California 90089, USA
E-mail: js.yoon@usc.edu
Dr. M. A. Meitl
Semprius Inc.
Durham, NC 27713, USA

Dr. M. A. Meitl, Dr. C. A. Bower
X-Celeprint (US) Inc.
Research Triangle Park
NC 27709, USA
Prof. J. A. Rogers
Department of Materials Science and Engineering
Frederick Seitz Materials Research Laboratory
Beckman Institute for Advanced Science and Technology
University of Illinois at Urbana-Champaign
Urbana, Illinois 61801, USA
E-mail: jrogers@illinois.edu

applications in photovoltaics and emissive display systems represent some of the most advanced examples.

2. Transfer Printing

Transfer printing involves the use of a soft elastomer with engineered features of relief on its surface (i.e., a soft stamp) for high speed, precision, nondestructive retrieval of spatially selected collections of micro- and nanostructured materials (i.e., solid 'inks') formed on a substrate (i.e., 'donor' substrate) for the purpose of delivery and distribution into two- and three-dimensionally organized arrays on a substrate of interest (i.e., 'receiver' substrate) in a massively parallel, deterministic manner (**Figure 1**a).[6–8] The 'ink' elements can be fabricated, for example, from high-quality bulk silicon, silicon-on-insulator (SOI), or epitaxially grown III–V compound semiconductors in schemes that involve anisotropic or selective wet chemical etching of underlying 'sacrificial' materials to release them from donor substrates. For the preparation of ink materials in printable forms, microfabricated structures (i.e., 'anchors') serve to retain lithographically defined layouts after undercut release.[7,11–13] Such strategies play critically important roles in the overall process. The details depend on the device architectures and constituent materials, as described separately in the different sections of this review.

Procedures of casting and curing elastomers such as poly(dimethylsiloxane) (PDMS) provide facile routes to stamps with features of relief whose dimensions can range from millimeters to nanometers.[14,15] The low modulus and low surface energy of PDMS allow soft, conformal contact against inks in which nonspecific van der Waals interactions typically dominate the adhesion.[6,7,9] Peeling back the stamp retrieves the ink elements by controlled microfracture at their anchoring points.[16] Contact against a target substrate followed by removal of the stamp delivers these elements to desired locations, thereby completing the process. High yields rely critically on methods that allow the adhesion strength to the stamp to be reversibly switched between high and low values, for the retrieval and delivery, respectively. One simple technique exploits velocity-dependent energy release rates ($G = F/w$, F: peeling force, w: width) between a viscoelastic stamp and a nonviscoelastic ink (Figure 1b).[9,16] Here, the critical energy release rate for steady-state crack propagation at the interface between the stamp and ink, $G_{crit}^{stamp/ink}$, is governed by the peeling velocity (v), while that at the interface between the ink and substrate, $G_{crit}^{ink/substrate}$, is independent of v. At high peeling rates, $G_{crit}^{stamp/ink}$ becomes greater than $G_{crit}^{ink/substrate}$, thereby leading to efficient retrieval of ink elements from the source substrate.[9,16] At low peeling rates, the energy release rate by the peeling action reaches the critical energy release rate for the stamp/ink interface first, for high yield delivery to the target substrate.[9,17,18] Advanced strategies that further improve the printing efficiency, of particular value for challenging cases (e.g., rough target substrate surfaces), include the use of pulsed laser illumination,[19,20] surface relief structures,[17,18] or the application of shear strains[21,22] (Figure 1c). The transfer yield can be also enhanced by exploiting specific interactions between the inks and the target substrate[23,24] or by adding thin layers of adhesive materials such as polyurethane,[12,25] polyimide,[13,26]

Jongseung Yoon obtained BS degree in polymer science from Seoul National University in 1996, and a PhD in Materials Science and Engineering from MIT in 2006. From 2007 to 2010, he was a Beckman Institute Postdoctoral Fellow at the Beckman Institute of Science and Technology at the University of Illinois at Urbana-Champaign. He is currently an Assistant Professor in the Department of Chemical Engineering and Materials Science at University of Southern California. He is a recipient of DARPA Young Faculty Award (2012) and Hanhwa Advanced Materials Non-Tenure Faculty Award (2015).

John A. Rogers obtained BA and BS degrees in chemistry and in physics from the University of Texas, Austin, in 1989. From MIT, he received SM degrees in physics and in chemistry in 1992 and a PhD in physical chemistry in 1995. From 1995 to 1997 he was a Junior Fellow in the Harvard University Society of Fellows. He 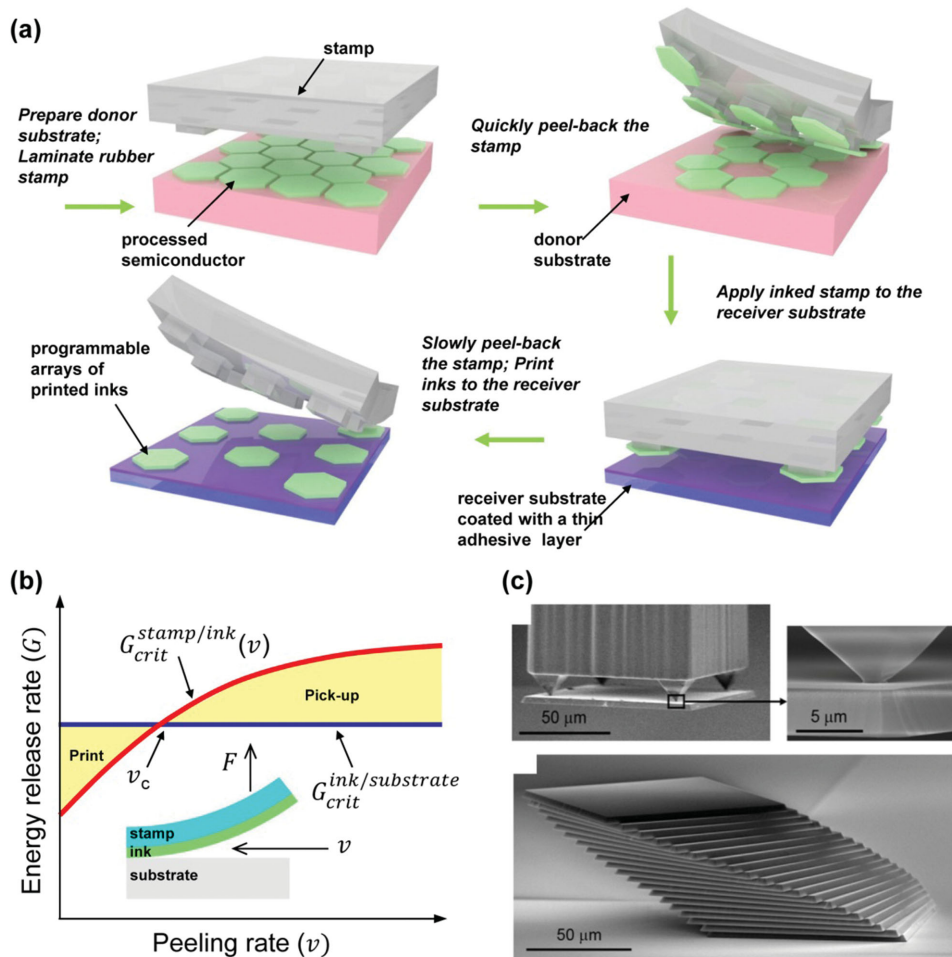joined Bell Laboratories in the Condensed Matter Physics Research Department in 1997, and served as Director of this department from the end of 2000 to 2002. He is currently Swanlund Chair Professor at University of Illinois at Urbana/Champaign, with a primary appointment in the Department of Materials Science and Engineering. He is a member of the National Academy of Engineering, the National Academy of Sciences and the American Academy of Arts and Sciences.

PDMS,[12,27] benzocyclobutene (BCB),[28,29] or epoxy resin.[30,31] Appropriate use of these approaches can enable yields that approach 100% for nearly any combination of ink, source, and target substrate. In-depth reviews on transfer printing can be found in the literature.[6,7] The following sections describe applications in optically active systems.
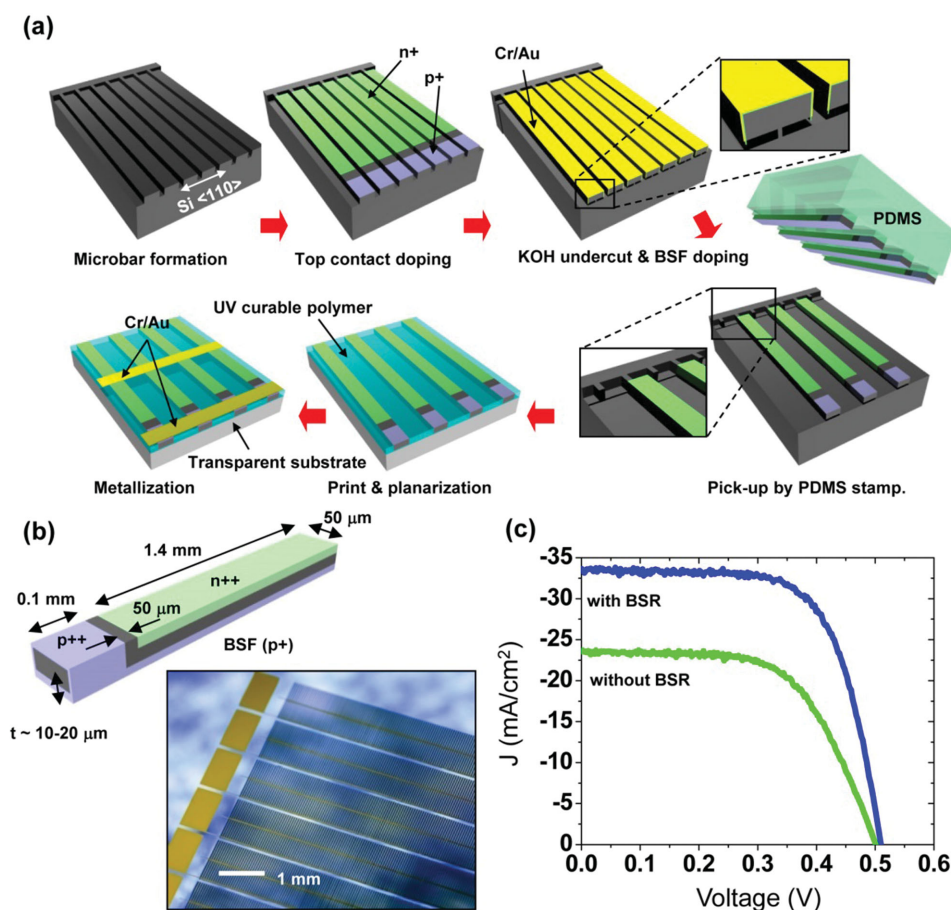
3. Solar Cells

3.1. Silicon Solar Cells

Crystalline silicon remains, by far, the most dominant semiconductor material for photovoltaics (PVs) due to its high natural

Materials
Views
www.MaterialsViews.com

ADVANCED
OPTICAL
MATERIALS
www.advopticalmat.de

REVIEW

Figure 1. a) Schematic illustration of the process flow for transfer printing with a soft, viscoelastic stamp. b) Schematic diagram of critical energy release rates for the ink/substrate interface ($G_{crit}^{ink/substrate}$) and for the stamp/ink interface ($G_{crit}^{stamp/ink}$). The intersection of the horizontal line (blue) with the curve (red) represents the critical peel velocity (v_c) for the kinetically controlled pick-up and printing processes. Reproduced with permission.[16] Copyright 2007, American Chemical Society. The inset illustrates the pick-up of the ink from the donor substrate by the stamp, where v and F are steady-state peel rate and peel force, respectively. c) Scanning electron microscope (SEM) images of an elastomeric stamp (top) with micro-tip designs and a stack of silicon platelets (bottom, $100 \times 100 \times 3$ µm^3) printed with small incremental rotations. Reproduced with permission.[18] Copyright 2010, The National Academy of Sciences.

abundance, self-passivating surface oxides, high refractive index, excellent transport properties, absorption across the solar spectrum, as well as compatibility with a production infrastructure that can scale to terawatt (TW)-level capacities.[32–34] The power conversion efficiencies of the most well developed commercially available silicon solar cells approach theoretical limits.[35] Further progress likely emerges from continued reductions in cost, where a value of ≈$0.50 W$_p^{-1}$ is generally believed to offer parity with conventional sources of grid power.[32,34,36,37] Research efforts in silicon photovoltaics tend now to focus on the development of concepts for improved efficiency in materials utilization, cost-effective manufacturing and/or unconventional module architectures. In this regard, ultrathin (compared to conventional cells) forms of single-crystalline silicon might provide routes to high performance, low cost photovoltaics, where carefully optimized designs could reduce the silicon consumption (≈50% of the total production cost in conventional silicon solar cells[32,34]) without decreasing the performance.

While various fabrication methods[38] exist for the production of thin-film single-crystalline silicon including epitaxial growth on porous silicon[39–42] and kerf-less exfoliation by stress-induced crack formation,[43–45] schemes based on anisotropic wet chemical etching[12,25,46–57] are of special interest due to their ability to generate a wide range of silicon thicknesses (e.g., ≈2–50 µm) from bulk wafers, without the need for additional silicon deposition steps. Suitable layouts yield microscale devices (i.e., microcells) in geometries that are compatible with transfer printing, as summarized in **Figure 2**.[12] The key idea involves spatially anisotropic etching rates that depend on crystallographic directions in single-crystalline silicon, for wet chemical etchants such as potassium hydroxide (KOH) and tetramethylammonium hydroxide (TMAH).[58–60] Fabrication begins with formation of trench-like structures on the surface of a silicon wafer with (111) orientation by photolithography and inductively coupled plasma reactive ion etching (ICP-RIE), such that the long axis of the trench aligns perpendicular to
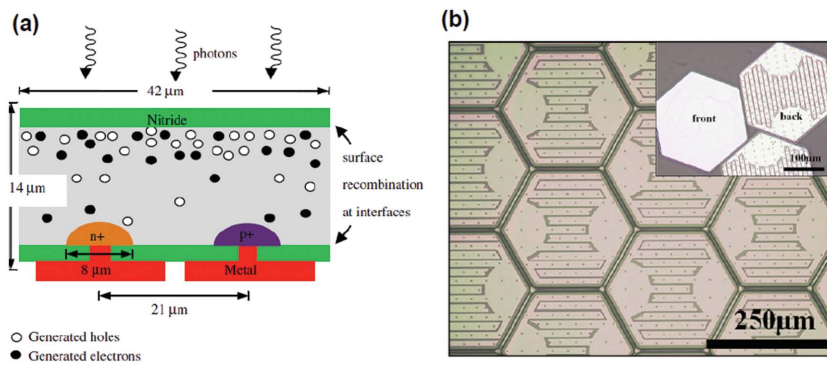
REVIEW

Figure 2. a) Schematic illustration of processes for fabricating ultrathin (≈15 μm) silicon solar microcells from a bulk (111) silicon wafer and assembling them into interconnected modules on a foreign substrate. b) Schematic illustration of a microcell that highlights the dimensions and the doping configurations. The inset shows a photograph of interconnected arrays of silicon microcells printed on glass. c) Representative current density (J)–voltage (V) curves from an individual microcell with thickness of 15 μm under AM1.5D illumination of 1000 W/m², with and without a white diffuse backside reflector (BSR). Reproduced with permission.[12] Copyright 2008, Nature Publishing Group.

the [110] direction of the silicon. In the next step, thermal diffusion of solid-state dopants of boron and phosphorous using lithographically patterned layers of silicon dioxide (SiO_2) and/or silicon nitride (Si_3N_4) as diffusion barriers define highly doped p- and n-type regions that can serve as electrical contacts to thin film metal electrodes and as the basis for a pn-junction. Subsequently, silicon dioxide (SiO_2) and/or silicon nitride (Si_3N_4) formed by plasma enhanced chemical vapor deposition (PECVD) protect the top surfaces and sidewalls during undercut etching. Reactive ion etching with masks formed by angled evaporation of metals (e.g., Cr) or photolithography selectively exposes silicon at the bottom surface of the trench, where the preferential etching of silicon in the [110] direction is initiated.[12,30,51] After lateral undercut etching in a hot (e.g., 100 °C) KOH solution, the exposed bottom surfaces of the microcells are doped by boron to form a back-surface field (BSF) that is electrically connected to heavily doped p-type regions on the top surface. Microcells released along their bottom surfaces remain tethered to the source wafer through narrow 'anchor' regions at their ends to maintain the lithographically defined arrangement.[16,30] In a related approach, similar anisotropic etching schemes can also produce 14 μm-thick microscale solar

cells with hexagonal shapes and point-contact doping layouts, in which surface passivation by PECVD silicon nitride enables 14.9% efficiency (**Figure 3**).[53,57,61]

All such types of microcells are compatible with transfer printing, as a practical means to manipulate and distribute them onto foreign substrates for module-level assemblies. Specifically, printing allows retrieval of entire collections or selective sets of completed microcells and their delivery onto substrates of interest in a precisely controlled manner at yields approaching 100%.[12,46,51] In some examples, a photocurable polymer (e.g., NOA) simultaneously serves as an adhesive layer for the printing and a planarizing medium that fills in the space between the microcells to facilitate the formation of metal interconnects by planar processes of thin film metallization. Repeating these steps with a given source wafer allows distribution of microcells over arbitrarily large areas on low cost substrates, at any desired coverage or layout. Experimental results indicate that efficiencies of microcells with thicknesses of ≈15 μm printed on glass substrates lie between ≈6–8% and ≈10–13% under AM1.5D illumination (1000 W m⁻²) without and with a back-side reflector (BSR), respectively.[12] Improved surface passivation and alternative configurations that use
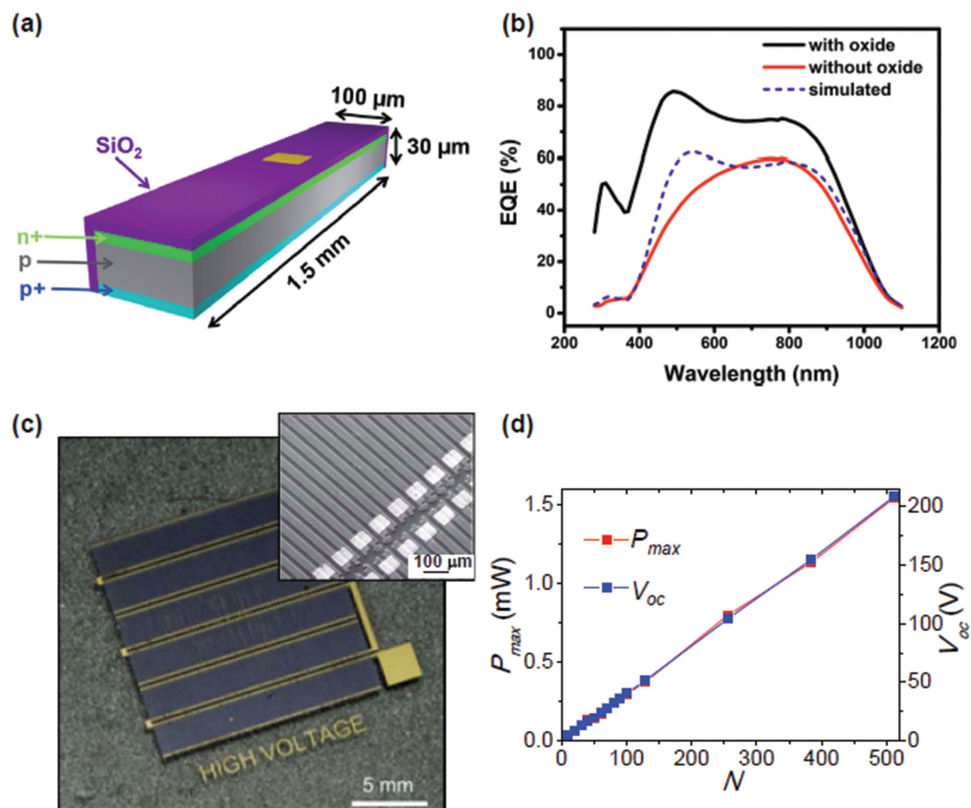
www.MaterialsViews.com

ADVANCED
OPTICAL
MATERIALS
www.advopticalmat.de

REVIEW

Figure 3. a) Representative 2D cross-sectional illustration of 14 μm-thick silicon solar cells, showing dopant profiles and recombination/generation sites. This block repeats 6 times in a 250 μm-wide solar cell. b) Top-view optical micrograph of arrays of such solar cells attached to a (111) bulk silicon wafer. Reproduced with permission.[53] Copyright 2011, Elsevier.
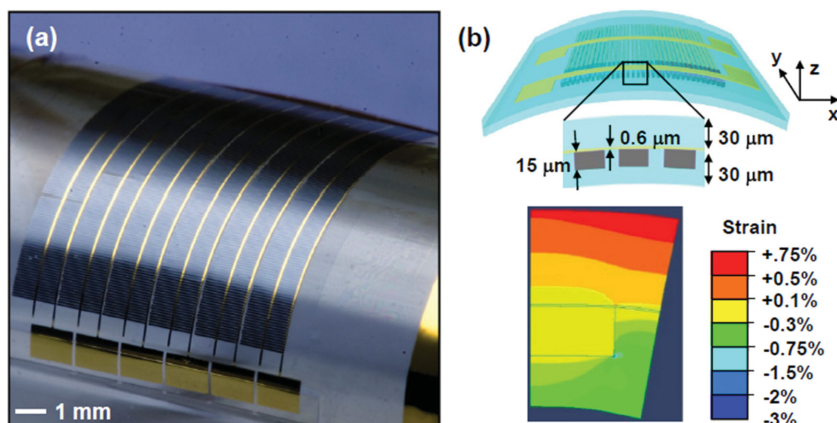
(e.g., anodized aluminium plates) exhibit one sun efficiencies of ≈12%.[25] Printed assemblies allow microcells to be interconnected in ways that can provide desired output characteristics in both current and voltage.[46,56] As an example that would be difficult to achieve in conventional designs, compact (≈0.95 cm × 0.63 cm) solar modules with high voltage (> ≈200 V) output are possible by series interconnection, where the output voltages scale with the number of interconnected microcells (Figure 4c,d).[46]

These schemes enable other options in module design that would be impossible with conventional cells and assembly methods. As an example, mechanically flexible solar modules result from arrays of silicon microcells printed onto sheets of polyethylene terephthalate (PET, thickness ≈50 μm), as in **Figure 5**.[12] Here, bendability follows from placement of the microcells near the neutral mechanical plane (NMP), as defined by the plane where bending-induced compressive and tensile strains cancel. A layer of polymer cast uniformly over the interconnected microcells places the NMP near the most fragile components (i.e., silicon) of the system, thereby effectively isolating them from

emitter and base contacts on the front and rear-surfaces of the microcells lead to enhanced efficiencies (**Figure 4**a,b).[25] Here, silicon dioxide (SiO_2) grown by wet oxidation serves as an antireflection coating (ARC), surface passivation layer and protective film for the undercut etching, as well as a diffusion barrier for the base boron doping. Resulting microcells with thicknesses of ≈30 μm measured on non-reflective surfaces

Figure 4. a) Schematic illustration of a microcell design with improved surface passivation using thermal oxide and a doping configuration that uses emitter and base contacts on the front and rear-surfaces of the microcells. b) External quantum efficiencies (EQEs) for silicon solar microcells with (black) and without (red) the thermal oxide layer. A simulated EQE curve (blue dashed line) for a non-passivated device with enhancements only from an AR coating is also shown. Reproduced with permission.[25] Copyright 2013, Royal Society of Chemistry. c) Photograph and SEM (right inset) image of a high-voltage photovoltaic module consisting of interconnected silicon microcells. d) Scaling properties for voltage (V_{oc}) and power outputs (P_{max}) with numbers of microcells interconnected in series. Reproduced with permission.[46] Copyright 2010, Royal Society of Chemistry.

Figure 5. a) Photograph of a mechanically bendable module constructed with silicon microcells. b) Color contour plot of calculated bending strains (ε_{xx}) through the cross section of a mechanically flexible module, bent along the cell width direction at R = 4.9 mm. The finite element modeling (FEM) calculations use symmetry boundary conditions for evaluating a single unit cell of the system. The black lines delineate the boundaries of the microcell and the metal interconnect line. Reproduced with permission.[12] Copyright 2008, Nature Publishing Group.
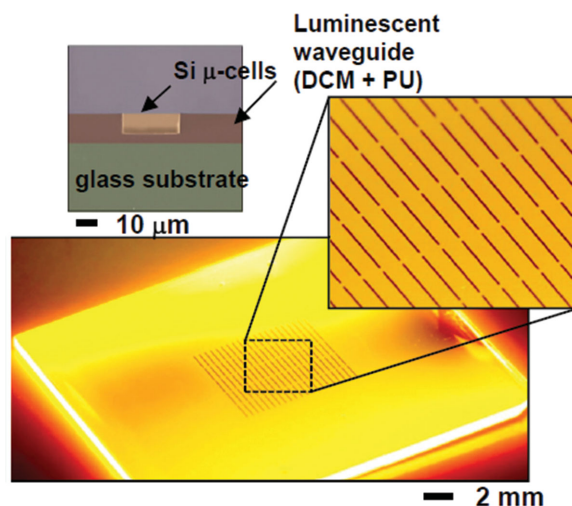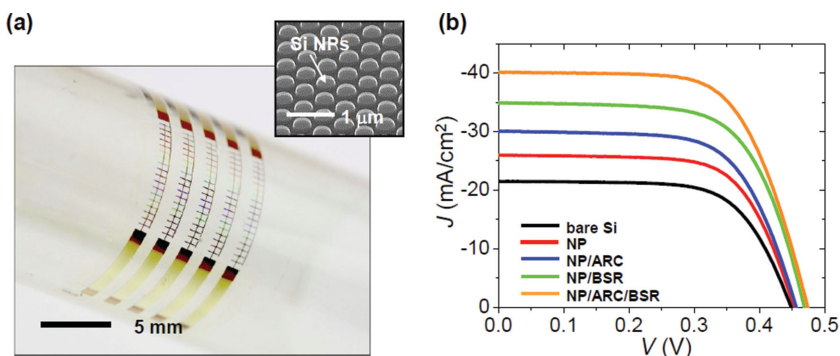
the design of a dielectric Bragg mirror as a front-surface light trapping structure with angle- and wavelength-averaged reflectivity exceeding 99%, which in turn produces concentration factors of nearly 100 even at their comparatively low luminescent quantum yields of ≈35%.[50]

These approaches in optical concentration are of interest due to their ability to maximize the utilization of the silicon.[68] Another strategy involves use of extremely thin microcells. As the silicon thickness decreases below ≈20 μm, the absorption of solar radiation decreases significantly due to the indirect bandgap in silicon.[69–71] In conventional, wafer-based cells, surface texturization induced by anisotropic wet chemical etching (e.g., in KOH or TMAH) can increase the optical path length in the silicon, thereby enhancing the absorption, although with feature sizes much too large for use in microcells.[72,73] Subwavelength diffractive nanostructures can, however, offer combined effects of antireflection, diffraction, and light trapping[47,51,74–77], suitable for application in microcells. Experimental demonstrations exploit light trapping structures (LTS) based on hexagonally periodic cylindrical nanoposts (e.g., period (P) = 500 nm, relief depth (RD) = 130 nm, diameter (D) = 350 nm) on the front surfaces of silicon microcells (≈6 μm).[47,49,51] Optimized choices for RD and D enable low reflection losses with maximum coupling of light into diffracted orders for effective trapping. 6-μm-thick microcells with LTS and antireflection coatings (ARCs) provide efficiency enhancements of ≈83% compared to the case of bare silicon.[47] Application to microcells with

strains due to bending.[12,62] As a result, the module performance remains invariant under repetitive bending to radii as small as ≈4.9 mm and for cycles of up to 200 times or more.[12] As another example, the spatial layouts of the microcells can be tailored to yield modules with any selected level of optical transparency, simply by adjusting the cell-to-cell spacings. Such sparse arrays of microcells can also be combined with molded cylindrical lens arrays to form low-profile micro-optic concentrator modules that further minimize the use of the silicon.[12,61]

Other unusual forms of concentration are also possible. For example, printed composite assemblies of silicon microcells, waveguides and luminophores allow the construction of an integrated type of luminescent solar concentrator (LSC) module.[48] In conventional LSCs, solar cells mount on the edges of a planar, multimode slab waveguide doped with luminophores that absorb incident light and re-emit longer wavelength photons in processes of optical down-shifting.[63,64] The emitted photons that satisfy the condition of total internal reflection (TIR) transport to the edges of the slab where they are captured by the edge-mounted cells. Despite attractive features such as the ability to concentrate diffuse light without the need for trackers, the performance of conventional LSCs suffers from optical inefficiencies associated with propagation losses due to absorption, scattering, and/or leaky waveguiding.[65,66] LSC designs enabled by transfer printing embed arrays of microcells directly in the waveguiding medium in spatial layouts that match the intrinsic loss characteristics (**Figure 6**).[48,67] In this approach, both direct (through the top surface of microcell) and indirect (through the sidewall and bottom surface of microcell) photon flux contribute to the output power, to enable improved collector efficiencies compared to those of conventional devices. Recent work shows that such LSC systems with CdSe/CdS nanorods as luminophores dispersed in UV-cured poly(lauryl methacrylate) matrices can be engineered to reduce the overlap of emission and absorption spectra (i.e., Stokes shift) and therefore the reabsorption of emitted photons.[50] The narrow linewidth of emission from nanorods also allows

Figure 6. Photograph of a luminescent solar concentrator system with an array of surface-embedded monocrystalline silicon solar cells. The inset shows a magnified image of microcells printed into a photocured layer of polyurethane doped with the luminophore, and a cross-sectional SEM image showing substrate (green), DCM-PU (red), silicon microcell (yellow), and air (blue). Reproduced with permission.[48] Copyright 2011, Nature Publishing Group.

www.MaterialsViews.com

ADVANCED
OPTICAL
MATERIALS

www.advopticalmat.de

REVIEW

Figure 7. a) Photograph of large-area, flexible solar modules composed of sparse arrays of interconnected nanostructured silicon microcells printed on a PET substrate, where angle-dependent diffractive colors can be seen. The inset shows a SEM image of hexagonally periodic silicon nanoposts implemented on the emitters of the microcells. b) Representative *J-V* curves of individual microcells for various configurations including cells constructed with bare silicon, with arrays of nanoposts (NP), with NP and antireflection coatings (ARC, TiO$_2$ 60 nm), with NP and back-surface reflectors (BSR), with NP and both ARC and BSR, respectively. The data were collected under the AM1.5G illumination with light is incident on the flat surface of the printed microcells to eliminate the metal shadowing. Reproduced with permission.[51] Copyright 2014, American Chemical Society.

thicknesses of just 3 μm with a bilayer ARC (Si$_x$N$_y$/SiO$_2$) and a silver backside reflector yield an integrated absorption of ≈77% of AM 1.5D illumination, due to the synergistic effects of LTS and Fabry–Perot cavity resonances.[49] The required relief structures can be formed by soft lithographic techniques[47,49,51] or, as in recent demonstrations, by block copolymer lithography in which an etch mask of silver islands also provides plasmonic augmentation of the absorption.[78] Further advances exploit schemes in which all such processing of photonic nanostructures occurs on the source wafer, before transfer to the module substrate. Examples of such nanostructured silicon microcells with thicknesses of ≈8 μm appear in **Figure 7**.[51] When printed on transparent substrates, these cells can accept illumination through either the front or rear surfaces. The configuration with nanoposts on the rear surface (i.e., light incident on the flat surface of microcell) eliminates shadowing losses associated with the metal interconnects and also reduces the angular dependence of the performance compared to cells with nanoposts on the front surface.[51]
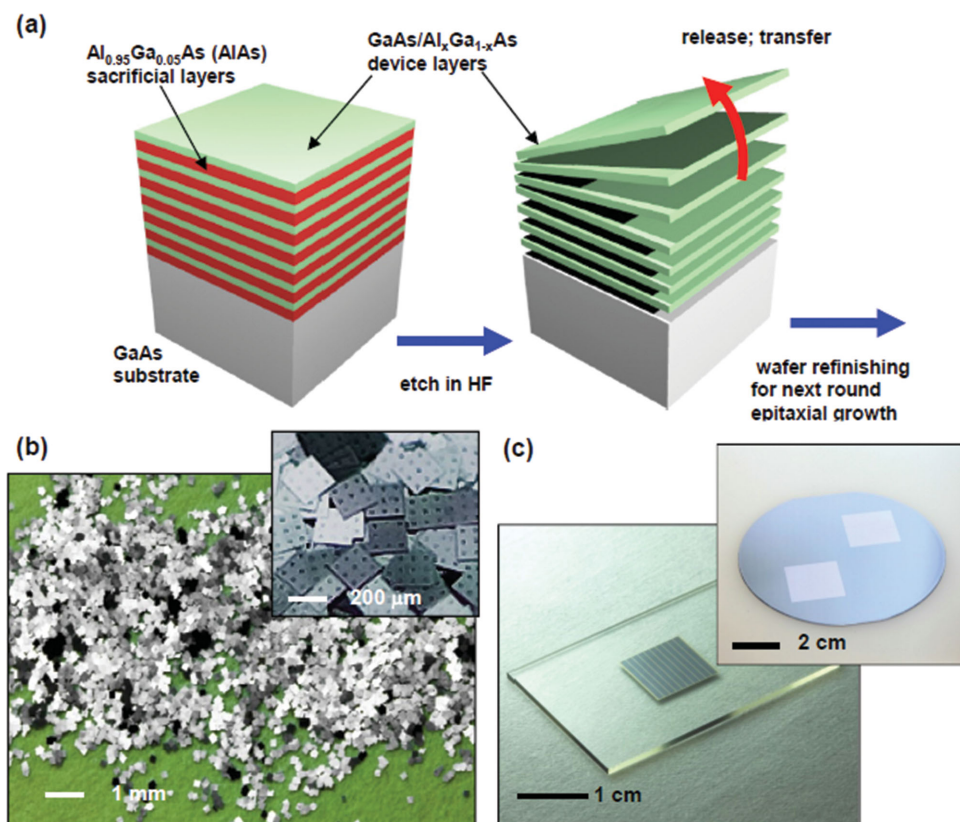
Another surface morphology that offers attractive features for photon management utilizes density-graded nanostructures (so-called 'black silicon') for broadband and omnidirectional antireflection and absorption enhancement[51,52,79–81], as demonstrated recently with printed silicon microcells.[51,52] Here, metal-assisted wet chemical etching of microcells (≈5.7 μm thickness) with an inverted doping layout forms density-graded rod-like nanocolumns on the front surface.[51] Another example uses HBr-based ICP RIE to yield nanocone structures on 30 μm-thick silicon microcells, where randomly dispersed oxide islands act as etch masks.[52]

3.2. III–V Solar Cells

III–V compound semiconductors serve as the basis for all ultrahigh efficiency solar cells due to their wide range of accessible bandgaps, high electron mobilities, and ability to form monolithic multi-junction devices.[82,83] The application of III–V solar cells is largely restricted to space missions, due to the prohibitively high costs associated with device-quality epitaxial materials.[84] Advances in processing and growth strategies have the potential, however, to improve the economics of III–V semiconductors in photovoltaics, and allow their competitive use in terrestrial systems. Recent work demonstrates that the concepts of transfer printing can be combined with single or multi-layer epitaxial liftoff (ELO) schemes to yield promising paths to unique classes of ultrahigh concentration modules, where many existing issues for the cost-competitive realization of III–V solar cells can be addressed.[13,67,85–93] The following sections summarize advances in materials, fabrication, and transfer printing strategies for III–V compound semiconductor solar cells.

The schemes of epitaxial liftoff, first pioneered by Konagai et al. in 1978,[94] enable the release of active epitaxial materials from a growth wafer by selective wet chemical etching of a sacrificial layer.[95–97] In the context of photovoltaics, the approach has been widely applied in various GaAs and InP based solar cells because of potential advantages in cost, arising from the substrate reuse and reduced materials consumption.[22,85,98–105] Despite progress over the past three decades, however, conventional ELO has not emerged as an economically viable strategy due to many challenges including materials degradation in wafer recycling, low throughput in undercut etching, as well as difficulties in handling the released materials. Many of these issues can be addressed by new ideas, coupled with the methods of transfer printing. A first example appears in **Figure 8** where the starting point is a thick, multilayer stack of device-grade material epitaxially grown on a GaAs wafer by metal organic chemical vapor deposition (MOCVD), with compositions, thicknesses, and dopant characteristics of each layer selected to satisfy specific application requirements.[13,87,88] Transfer printing allows the sequential retrieval of individual device layers following release by selective wet chemical etching of embedded sacrificial layers (e.g., AlAs for the case of GaAs). Printing-based delivery and distribution in a step-and-repeat manner to substrates of interest represents a critical step toward large-area, low cost modules. This concept of releasable multilayer assemblies relaxes stringent requirements of wafer reuse (e.g., >100 times) in conventional, single-layer epitaxial liftoff (ELO)[84] and greatly improves the utilization of growth tools by eliminating cycles for load/unload, both of which, taken together, contribute to a significant fraction of the overall fabrication cost of III-V solar cells. Early demonstrations involved 'n-on-p' type GaAs single-junction solar cells epitaxially grown in triple-stack assemblies with zinc and silicon as the p- and n-type dopants, respectively.[13] Arrays of microscale (≈500 × 500 μm^2) solar cells from each device stack follow from delineation of the cell layout by wet chemical etching and

REVIEW

ADVANCED
OPTICAL
MATERIALS
www.advopticalmat.de
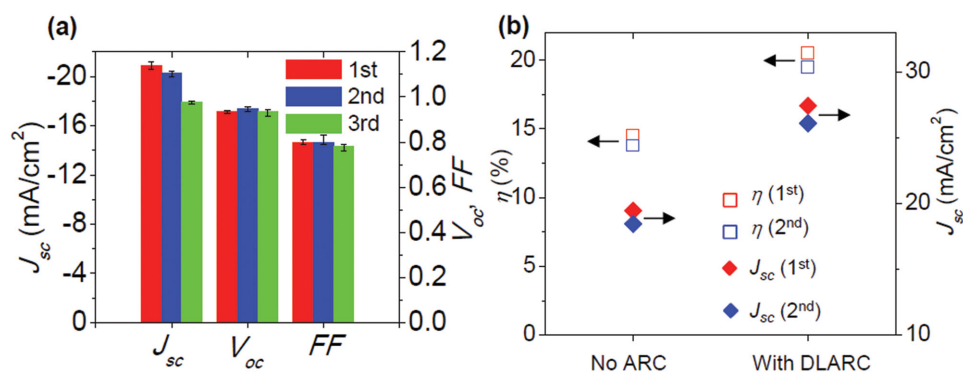
Materials
Views
www.MaterialsViews.com

Figure 8. a) Schematic illustration of a multilayer stack of GaAs/AlAs and schemes for release through selective etching of the AlAs. b) Photograph of a large collection of GaAs solar cells formed by release from a three-layer stack, and then solution casting onto another substrate. The inset shows a high magnification view. c) Photograph of a GaAs solar cell with a size of ≈10 × 10 mm² printed on a glass substrate with no ARC. The inset shows a photograph of GaAs solar cells with sizes of ≈25.4 × 25.4 mm² printed on a Si substrate. Reproduced with permission.[13] Copyright 2010, Nature Publishing Group.

formation of coplanar p- and n-type ohmic contacts by metal evaporation and liftoff processes. Unlike silicon solar cells with 'homogeneous' (i.e., silicon) anchor designs as described in the previous section, polymeric (e.g., photoresist) 'heterogeneous' anchor structures hold the released devices in the array configuration after complete undercut etching. The projected one-sun (AM1.5D, 1000 W m^{-2}) efficiencies of the multilayer-grown GaAs solar cells based on the experimentally measured external quantum efficiency (EQE) and a double layer antireflection coating (e.g., MgF$_2$/ZnS) are 20.5% and 19.5%, respectively, for devices formed with material from the top and middle layers of the stacks (**Figure 9**). Recent, alternative epitaxial designs eliminate mobile dopants, such as Zn, in the multilayer growth.[87,88] For example, using carbon instead of Zn as a p-type dopant in a 'p-on-n' configuration minimizes such effects.[87] Further improvements in Zn-doped triple-stack assemblies are possible by exploiting Ga$_{0.50}$In$_{0.50}$P as a window and BSF layers in a p-on-n device configuration.[88]

These thin film (< ≈5 µm) III–V materials can yield high performance solar cells with attractive options in integration and module designs that cannot be realized in other ways, with significant benefits in cost and performance. As with silicon microcells, output characteristics of modules comprising printed arrays of GaAs microcells can be configured to meet the requirements of specific applications by adjusting

the layouts of parallel- or series-connected microcells.[13,67,85] Mechanically bendable or stretchable modules are also possible by heterogeneously integrating collections of microcells onto thin sheets of plastic or slabs of microstructured rubber, respectively.[13,85,86,88] As in the case of silicon, NMP designs reduce the bending induced strains in the GaAs in flexible modules (**Figure 10**a).[13,85,86] Systems that can accommodate not only bending but also stretching and twisting, with high areal coverage of microcells (e.g., ≈70%) are possible by use of structured elastomeric substrates that have isolated raised regions separated by recessed trenches (Figure 10b).[85] Here, arrays of single-junction GaAs microcells (≈760 × 760 µm²) interconnected by flexible, ribbon-type structures reside on the raised regions. At an overall strain of ≈20%, the trench regions (≈156 µm wide) experience large extension (≈123%), thereby absorbing most of the externally applied strains, while the islands (≈800 × 800 µm²) barely deform (≈0.4%).[85] An enhanced version of this type of structure incorporates rectangular notches in the central regions of the edges of the islands to impart both strain-isolation and strain-limiting behaviors.[86] Demonstrations with 19%-efficiency GaInP/GaAs dual junction solar microcells at a high (≈67%) areal coverage illustrate that the notches effectively increase the length of interconnect lines, which in turn reduces the imposed strain and hence increases the overall stretchability compared to cases without notches.[86]
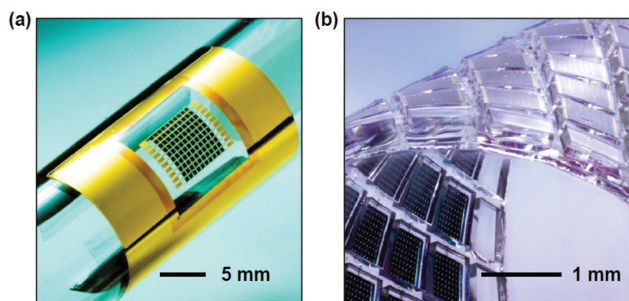
Materials
Views
www.MaterialsViews.com

ADVANCED
OPTICAL
MATERIALS
www.advopticalmat.de

REVIEW

Figure 9. a) Short-circuit current density (J_{sc}), fill factor (FF), and open circuit voltage (V_{oc}) of devices derived from the first, second, and third layers in multilayer stacks grown on a source wafer. b) Projected efficiencies (η) and J_{sc} values without ARC and with double-layer ARC (DLARC; MgF$_2$/ZnS) for devices formed using materials from the first and second layers. Reproduced with permission.[13] Copyright 2010, Nature Publishing Group.
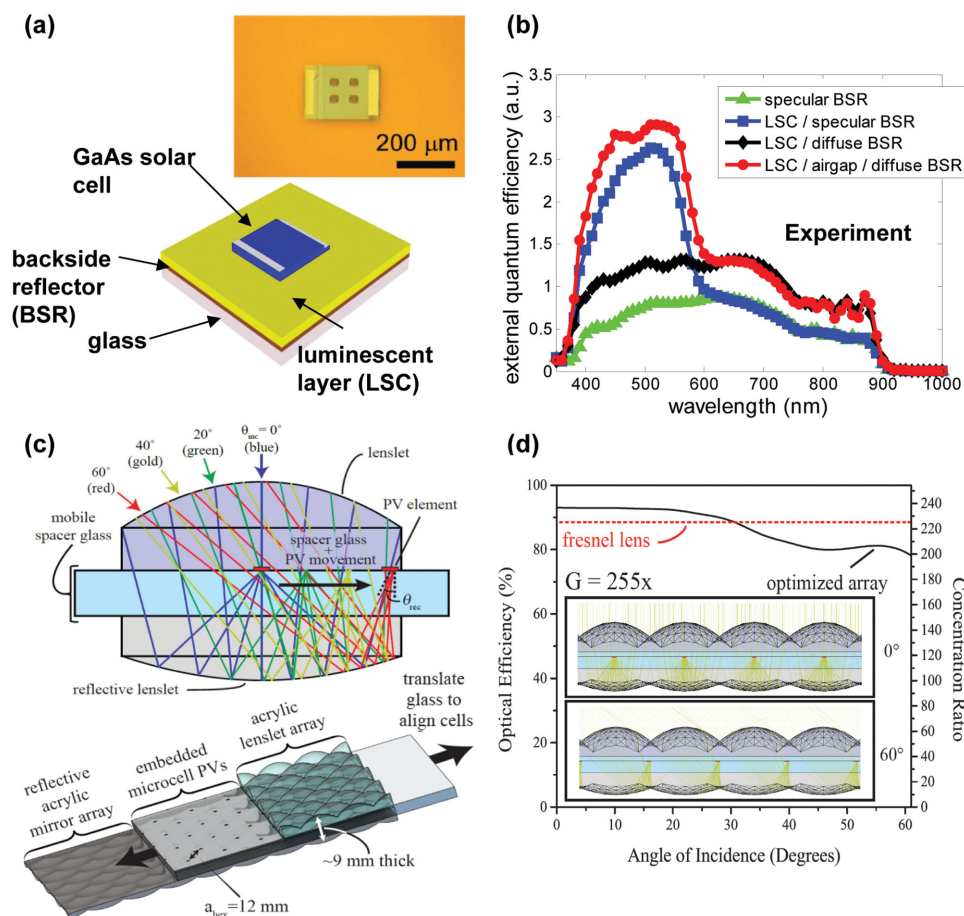
This layout also offers a strain-limiting capability, in which spaces remain for interconnects even at levels of deformation (e.g., inward bending) that cause physical contact of the top-surface edges of the islands.

As with silicon, transfer printed GaAs microcells can be used in unusual concentrator designs. In one example, integration of bifacial GaAs microcells (240 × 200 μm^2) into LSCs improves the power output (**Figure 11**a,b).[67] Here, additional enhancements follow from optimized use of reflective elements placed underneath the luminescent medium. In particular, a diffuse BSR, placed with a small air gap between the LSC increases the short circuit current density (J_{sc}) by nearly a factor of two, due to enhanced photon capture from broadband scattering, without any reduction in the waveguiding effect.[67] In another case, wide-angle planar microtracking concentrator modules capable of maintaining >200-fold increase in power output (compared to an unconcentrated cell) for incidence angles ranging ±60° follow from embedding GaAs microcells between a pair of plastic lenslet arrays (Figure 11c,d).[91] A folded optical path configuration that combines refraction from a convex front surface with reflection from a concave rear surface virtually eliminates the Petzval curvature and produces an intermediate focal plane between the two, where a small (<1 cm) lateral translation at fixed latitude tilt enables full-day tracking with >200× flux concentration ratio.

Single-junction solar cells suffer from inefficiencies related to thermalization of absorbed photons with energies higher than the bandgap, as well as inability to capture photons with energies lower than the bandgap.[106,107] These and other effects are captured in the Shockley–Queisser limit on performance of single-junction cells.[106] Monolithically grown multijunction solar cells represent the most highly explored route to efficiencies that bypass these limits.[82,83,89,108] Stringent requirements on lattice and current matching represent daunting challenges that restrict the application of such cell architectures to a narrow range of materials systems and a relatively small number of junctions.[82,83,109] Mechanical stacking of separately grown cells represents an alternative route to multijunction devices, without any intrinsic limit on materials types or numbers of junctions.[110–114] Practical difficulties associated with wafer bonding, interface management and others have, however, prevented any commercial use of stacking, in spite of decades of effort in this direction. Transfer printing, combined with high index, dielectric interface layers, offers an attractive alternative to previous attempts. Recent experiments demonstrate four-terminal, quadruple-junction cells formed in this manner and their use in high concentration modules, including on-sun evaluation (**Figure 12**).[89] Here, triple-junction InGaP/GaAs/InGaAsNSb stacks designed with a sacrificial layer for ELO serve as inks for transfer printing onto diffused-junction Ge solar cells to form deterministically assembled quadruple-junction cells, with efficiencies of 43.9% at concentrations exceeding 1000 suns. A key in this architecture is a layer of As$_2$Se$_3$ as an interfacial material between the top III–V and bottom Ge solar cells, that offers high breakdown strength, high thermal conductivity, optical transparency in the infrared wavelength, and refractive index (≈2.7) similar to the adjacent semiconductors to minimize reflection losses and barriers to thermal transport. Such transfer printed multi-junction microcells have been exploited in pilot-scale commercial concentrator modules with certified efficiencies of 35.5% (**Figure 13**), where arrays of microcells printed on a ceramic submount substrate integrate with two-stage, low profile optical designs composed of primary silicone-on-glass plano-convex lenses and secondary ball lenses to produce geometrical concentration ratios exceeding 1000.[115,116]

Figure 10. a) Photograph of a solar module consisting of a 10 × 10 array of GaAs microcells on a PET substrate. Reproduced with permission.[13] Copyright 2010, Nature Publishing Group. b) Photograph of stretchable GaAs solar module formed on a structured PDMS substrate. Reproduced with permission.[85] Copyright 2011, John Wiley & Sons.

ADVANCED
OPTICAL
MATERIALS
www.advopticalmat.de

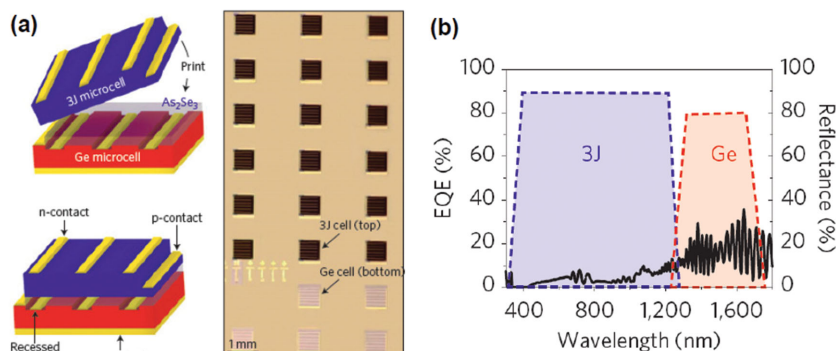REVIEW

www.MaterialsViews.com

Figure 11. a) Schematic illustration of a GaAs microcell transfer printed onto a luminescent solar concentrator (LSC) layer, with a backside reflector (BSR) on the surface of a supporting glass substrate. The upper inset shows an optical micrograph of a GaAs microcell (200 × 200 μm²) with four holes to facilitate epitaxial liftoff, and metallic ohmic contacts, printed on an LSC substrate. b) Measured EQE spectra of printed GaAs microcell at various LSC substrate configurations including polyurethane (PU)/specular BSR (green triangle), LSC/specular BSR (blue square), LSC/diffuse BSR (black diamond), and LSC/air gap/diffuse BSR (red circle). Reproduced with permission.[67] Copyright 2013, John Wiley & Sons. c) Schematic illustration of a microtracking microcell CPV panel. An array of microcells transfer-printed on a central acrylic sheet tracks the sun by sliding laterally between stationary upper and lower acrylic lenslet arrays lubricated by index matching oil. The upper inset shows a ray-tracing schematic illustration of the elimination of Petzval curvature through use of a folded optical path, where the focal plane lies in the middle of a dielectric with refractive upper and reflective lower surfaces. d) Simulated absolute optical efficiency of the array in (c), defined as the fraction of incident optical power in the AM1.5D solar spectrum delivered to the surface of the microcell, where the microcell dimensions are 0.7 × 0.7 mm², and the lattice constant of the lenslet array is 12 mm, yielding a nominal geometric gain G = 255. Reproduced with permission.[91] Copyright 2015, Nature Publishing Group.

3.3. Organic Solar Cells

For organic or polymeric photovoltaic devices (OPVs), solution-based fabrication methods such as spin-coating or screen printing offer high throughput, low cost, and large-area processibility.[117–119] However, construction of multilayer device structures with controllable, well-defined materials interfaces and geometrical patterns is often demanding in such wet deposition processes due to the requirements of solvent orthogonality[120,121] and intrinsic immiscibility between dissimilar conjugated polymers.[122,123] In this context, transfer printing offers complementary fabrication pathways for multilayered architectures in organic solar cells, for enhanced performance as well as expanded choices of materials combinations, compositions and spatial organizations.[124–131] In one example, bilayer solar cells composed of poly(3-hexyl thiophene) (P3HT):[6,6]-phenyl C61-butyric acid methyl ester (PCBM) formed by transfer printing in ambient conditions offer improved rectifying behavior compared to devices that use blends, due to an increased shunt resistance.[124] More recently, experiments show that transfer printing allows facile control over a vertical compositional gradient in P3HT:PCBM active layers to increase the power conversion efficiency by ≈23%.[127] Here, a solution of P3HT and PCBM in chlorobenzene spin-cast on a UV/ozone treated silicon wafer yields a layer in which the hydrophilic PCBM resides near the silicon surface. A two-step transfer printing process with the resulting film results in solar cells with P3HT- and PCBM-rich active layers at the interface with MoO_3 anode and Ca/Al cathode, respectively, to improve the charge collection at the electrodes.[127]

www.MaterialsViews.com

ADVANCED
OPTICAL
MATERIALS
www.advopticalmat.de

REVIEW

Figure 12. a) Schematic illustration of a cell from a 3J thin-film stack of InGaP/GaAs/InGaAsNSb derived from epitaxial growth and liftoff and a separate 1J Ge cell, before (upper) and after (lower) assembly by transfer printing. The As$_2$Se$_3$ layer (light blue) and the recessed metal contact lines on the top of the Ge cell ensure excellent optical, electrical, and thermal properties at the interface. The right inset shows an optical micrograph of an array of 3J/Ge microscale solar cells. b) Schematic illustrations of the EQE and measurement of the reflectance spectra of a 3J/Ge cell. Reproduced with permission.[89] Copyright 2014, Nature Publishing Group.
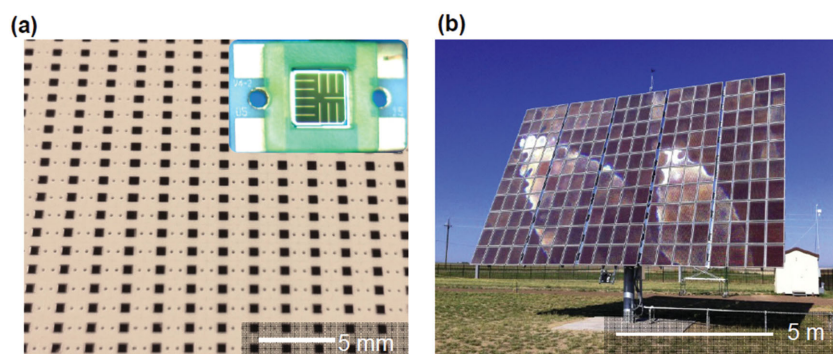
4. Light-Emitting Devices

4.1. Inorganic Light-Emitting Diodes

Inorganic light-emitting diodes (referred to here as ILEDs to highlight the distinction over organic light emitting diodes, OLEDs) represent a ubiquitous technology with widespread importance in nearly all lighting applications, from residential general illumination, to traffic signals, digital billboards, display backlights, portable light sources and others. The performance characteristics involve a combination of brightness, lifetime, and color purity that make ILEDs attractive compared to nearly any other option, including incandescent light bulbs, fluorescent lamps and OLEDs.[132,133] The vast majority of commercial applications of ILEDs rely on millimeter scale dies produced by wafer-dicing, robotic pick-and-place, and wire bonding, thereby imposing fundamental limitations on the device sizes, spatial densities in arrays, form factors, levels of power, and efficiency of materials utilization. Techniques of release and transfer printing, similar conceptually to those described in previous sections, lead to classes of ILEDs and their heterogeneous
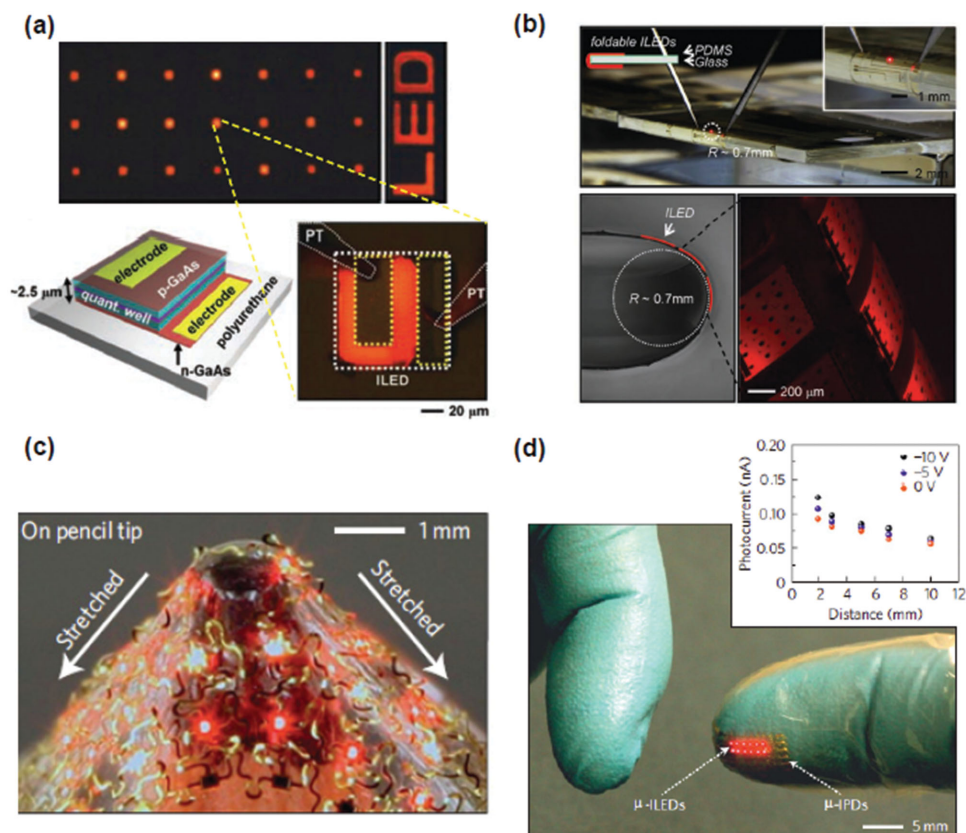
assemblies that circumvent restrictions of conventional systems, with diverse options in devices, ranging from high resolution flexible displays to cellular-scale, biocompatible light sources.[11,24,27,29,31,134–136] This section provides an overview of recent advances in this direction with a focus on materials designs and fabrication concepts for microscale ILEDs (μ-ILEDs), including foundational studies of the thermal and mechanical properties, as well as circuit- and system-level demonstrations in various unconventional areas of application.

As with the other compound semiconductors devices covered in this review, transfer printing of ILEDs requires specialized designs and processing steps that permit the separation and release of active materials from a growth wafer. The first demonstration of transfer-printed ILEDs involved red-emitting epitaxial materials based on AlInGaP-based quantum wells (i.e., In$_{0.56}$Ga$_{0.44}$P wells (6 nm)/ Al$_{0.25}$Ga$_{0.25}$In$_{0.5}$P barriers (6 nm)) (**Figure 14**a).[27] Microscale (e.g., $\leq 250 \times 250$ μm^2) device layouts with coplanar[27] or vertical[135] contact configurations follow from photolithography and combinations of dry and wet etching processes. After undercut etching of a sacrificial layer (Al$_{0.96}$Ga$_{0.04}$As), the isolated device arrays remain tethered to the GaAs source wafer by 'breakable' polymeric (e.g. photoresist) anchor structures.[27,135] Transfer printing allows selective retrieval of μ-ILEDs and their delivery to substrates of interest, sometimes facilitated by use of thin layers of photo- or thermally curable polymer adhesives. As in printed III–V solar cells, the small thicknesses (≈ 2.7 μm) of such μ-ILEDs allow planar processing to define electrical interconnects for large-scale arrays in lighting elements or addressable displays, where materials ranging from thin films of conventional metals [27,31,135,137] to graphene[134] serve as electrodes and conducting elements.

Such printing-based assemblies of μ-ILEDs provide radically different design options compared to those associated with conventional, large, thick devices that must be packaged individually with wire-bonds and serial, robotic pick and place operations. One of the most enabling examples is in the use of μ-ILEDs on mechanically flexible or even stretchable substrates. Such device platforms are potentially useful for building conformal displays and/or lighting systems that can be intimately integrated with soft, curvilinear surfaces such as those of biological tissues. Concepts similar to the ones discussed in the context of solar modules apply to μ-ILEDs, where the devices can be placed at the NMP[12,62,137] to eliminate strains in the quantum well, and associated changes in the emission wavelength from shifts in the bandgap. Careful studies of flexible AlInGaP μ-ILEDs in representative devices reveal that bending-induced tensile and compressive strains in the quantum

Figure 13. a) Photograph of transfer-printed multijunction GaAs solar cells on a low cost ceramic sub-mount substrate. The inset shows a magnified view. b) 64 m^2 single-tracker system installed in the Southwest USA, composed of 200 modules and 132 000 transfer-printed multijunction microcells. Reproduced with permission. Copyright 2015, Semprius Inc.
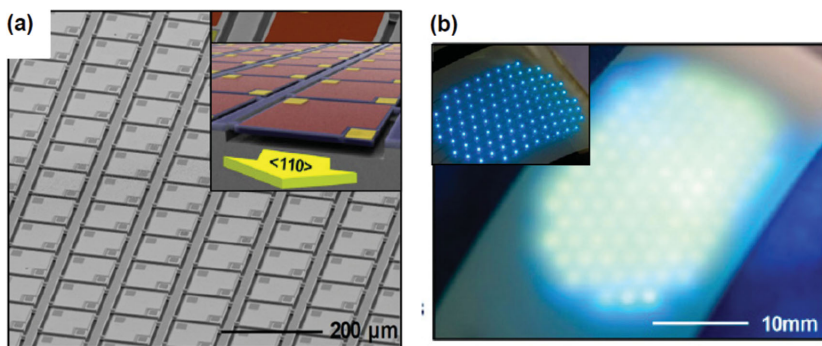
Figure 14. a) Optical micrographs of an array of microscale AlGaInP inorganic light emitting diodes (μ-ILEDs) (left: 25 μm × 25 μm, square geometries; right: characters "LED") in their on state. Schematic illustration (bottom left) of an ILED with integrated ohmic contacts and optical image (bottom right) of an operating device. Reproduced with permission.[27] Copyright 2009, The American Association for Advancement of Science. b) Optical images (top) of μ-ILEDs (100 × 100 μm²) in a neutral mechanical plane layout, during operation wrapped around the edge of a slide glass (1 mm thick). The bending radius is <0.7 mm. Cross-sectional optical image (bottom left) of a similar μ-ILED system and composite magnified view (bottom right) to show bending in the individual devices. Reproduced with permission.[137] Copyright 2013, John Wiley & Sons. c) Photograph of a 6 × 6 array of μ-ILEDs, tightly stretched on the sharp tip of a pencil. d) Photograph of a 4 × 6 array of μ-ILEDs with serpentine metal bridges, transfer-printed on the fingertip region of a vinyl glove. The inset shows a plot of photocurrent as a function of distance between the sensor and an object (white filter paper) for different reverse biases and different voltages. Reproduced with permission.[31] Copyright 2010, Nature Publishing Group.

wells yield red- (Δλ ≈ +1.77 nm) and blue-shifts (Δλ ≈ −1.27 nm) of emission wavelengths, at bending radii of 4.9 and 5.4 mm, respectively.[137] With NMP layouts, the systems remain functional even after bending to form sharp folds with bending radii of ≈0.7 mm (Figure 14b).[137]

Conformal integration of μ-ILEDs on curvilinear, deformable surfaces such as human skin or internal organs demand constructs that can accommodate more complex deformation modes than simple bending, including high degrees of stretching.[27,31] Building on recent advances in flexible electronics, stretchable μ-ILEDs can be achieved by dual transfer printing.[27,31,134,138] In this process, release of fully-functional μ-ILEDs formed on a source wafer and delivery to a temporary glass substrate coated with a trilayer of epoxy (SU-8)-polyimide-poly(methyl methacrylate) (PMMA) allows formation of serpentine-shaped ribbons that serve as both structural bridges and electrical interconnects. Interconnected arrays of μ-ILEDs fabricated in this way can be released from the glass by dissolving a sacrificial coating (e.g., PMMA), to allow a second transfer printing operation for integration on a pre-strained sheet of elastomer (e.g., PDMS) through selective bonding at

the locations of the devices. Release of the pre-strain yields non-coplanar layouts in the serpentine metal interconnects through nonlinear buckling physics.[27,31] The resulting device platform is mechanically robust, with stable operation over a wide range of deformation modes including uniaxial, biaxial, shear, twisting, and other mixed forms, without any appreciable changes in the performance (Figure 14c).[31] Here, the non-coplanar interconnects accommodate the great majority of the deformation, such that the maximum strains in the device components remain well below their linear elastic limit.[31,134] Such favorable mechanical attributes of flexible assemblies of μ-ILEDs together with biocompatible and water-proof packaging schemes enable their intimate integration with the organs of the human body as well as the creation of unusual classes of optical sensors. An example of the former is in arrays of red μ-ILEDs integrated on balloon catheters for highly localized photodynamic drug delivery and activation, phototheraphy, or spectroscopic characterization of tissue disorders.[138] In another demonstration, an array (1×4) of red μ-ILEDs mounted on PDMS-coated cotton or nylon threads act as light-emitting sutures for accelerated healing, where a fully encapsulating

www.MaterialsViews.com

ADVANCED
OPTICAL
MATERIALS
www.advopticalmat.de

REVIEW

Figure 15. a) SEM image of a dense array of InGaN µ-ILEDs on a Si (111) wafer after aniso-tropic etching of the near-interfacial region of a Si wafer. The inset shows a schematic illustration of the preferential direction for anisotropic wet chemical etching with KOH. b) Optical images of a fully interconnected array of InGaN µ-ILEDs with a laminated film of encapsulated YAG:Ce phosphor islands (500 × 500 µm²) and a diffuser film. The inset shows the corresponding printed ILEDs. Reproduced with permission.[29] Copyright 2011, The National Academy of Sciences.

layer of PDMS provides a soft, elastomeric, and biocompatible barrier to the surrounding tissue and biofluids for deep-tissue applications.[31,138]

Flexible and stretchable µ-ILEDs also find use as light sources in unusual classes of integrated optical sensors. Stretchable arrays of µ-ILEDs can be integrated with thin, molded plasmonic crystals as refractive-index microsensors for use in intravenous delivery systems, in which transmission of light from µ-ILEDs can be correlated to variations in refractive index of the surrounding fluid.[31] In a different example, water-proof µ-ILEDs and microscale inorganic photodetectors (µ-IPDs) co-integrated onto the fingertip of a glove,[31] can be used as an optical proximity sensor (Figure 14d).
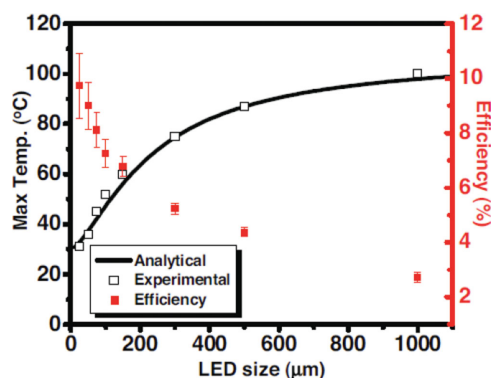
A conceptually similar set of release and transfer printing protocols work well with blue ILEDs. Here, the interest is in devices based on indium gallium nitride (InGaN) for energy-efficient solid-state lighting due to significantly higher luminous efficacies (>200 lm W⁻¹) than those possible with conventional triphosphor fluorescent lamps (e.g., ≈90 lm W⁻¹).[139,140] As with the AlInGaP devices described previously, transfer printing offers an effective route to thin, lightweight, and large-area emissive platforms comprising collections of ultrathin, small InGaN LEDs. Procedures exist for using epitaxial materials grown on silicon or on sapphire.[11,24,29,141–143] Silicon substrates are of interest due to their potential for advantages in cost and throughput of materials growth compared to sapphire or silicon carbide (SiC).[144] Silicon also offers simple release schemes based on anisotropic wet chemical etching of silicon by KOH or TMAH, similar to those used for silicon solar microcells.[29,145,146] In this way, fully-formed arrays of µ-ILEDs in freely suspended configurations can be designed in 'print-ready' forms (**Figure 15**a). The large bandgap of GaN (≈3.4 eV, 365 nm) allows a remarkably simple process to open the contact regions for the metal interconnection without the need for lithographic patterning. Here, H-line radiation (≈405 nm) that illuminates the system from the backside of a transparent substrate (e.g., glass or plastic) passes through all regions except those shadowed by the metal contacts, to photocure a planarizing polymer over-coat everywhere except

at the contact regions.[29] Washing the uncured material away prepares the substrate for photolithographic definition of interconnects, to complete the fabrication. Uniformly emissive lighting modules can be formed from such devices by a laminating a sheet of PDMS with cerium-doped yttrium aluminium garnet phosphors and a diffuser film (Figure 15b).[29,146]
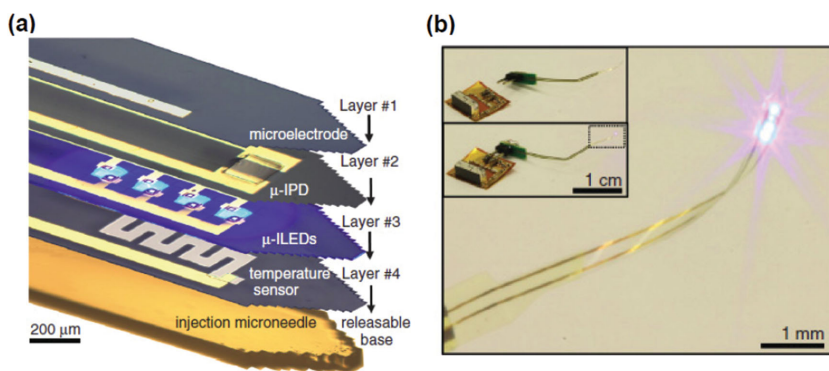
Fabrication routes to printable InGaN µ-ILEDs are also available for material grown on sapphire.[11,24,141–143] The release operates on fully formed arrays of µ-ILEDs, wafer bonded to a temporary silicon substrate using In-Pd alloys for interface adhesion. Conventional laser liftoff then releases the sapphire substrate to yield inverted µ-ILEDs on the silicon wafer. Dual transfer printing flips the devices over and selectively delivers them to a target substrate.[11,24,141] More recently, transfer-printed InGaN µ-LEDs based on 300-nm-thick nanomembranes have been obtained using conductivity-selective electrochemical etching,[147] where heavily doped n⁺-GaN as an anode is selectively removed by an HF-based etchant (HF/glycerol/ethanol). In another approach, 3-nm-thick single-crystalline hexagonal boron nitride (h-BN) serves as a release material that can be laterally fractured by mechanical shear force to allow liftoff of InGaN LED structures grown on sapphire, where AlN is used as a buffer layer to reduce the density of threading dislocations in the overlying InGaN materials.[148,149]

In all cases of µ-ILEDs, the ultra-small, thin device geometries together with the high thermal conductivity of the metal interconnects yield advantages in thermal management. The rates of passive heat spreading scale favorably with device size, which is enabling for their reliable operation on substrates with low to moderate thermal conductivities such as plastics or biological tissues (**Figure 16**).[11,29,150,151] Moreover, the metal lines serve dual roles as electrical interconnects as well as efficient heat sinks due to their high thermal mass, compared to the µ-ILEDs, and thermal conductivities.[11,29] Combined theoretical

Figure 16. Measured (black symbol) and simulated (black line) maximum temperature as a function of InGaN µ-ILED size (lateral dimension) printed on a 50 µm-thick PET substrate, at 160 mW mm⁻². Red symbols show radiant efficiencies. Reproduced with permission.[151] Copyright 2012, John Wiley & Sons.

**ADVANCED
OPTICAL
MATERIALS**

www.advopticalmat.de

Materials Views

www.MaterialsViews.com

REVIEW

Figure 17. a) A multifunctional, implantable optoelectronic device, in a tilted exploded view layout illustrating various components. The system includes layers for electrophysiological measurement (no. 1: Pt contact pad, microelectrode), optical measurement (no. 2: silicon μ-IPD), optical stimulation (no. 3: μ-ILED array), and temperature sensing (no. 4: serpentine Pt resistor), all bonded to a releasable structural support for injection (microneedle). b) Integrated system wirelessly powered with RF scavenging. The insets show a connectorized device unplugged (top) and plugged into (bottom) the wireless power system. Reproduced with permission.[24] Copyright 2013, The American Association for Advancement of Science.

and experimental studies reveal the effects for μ-ILEDs printed on PET substrates.[11,29,136,152]

The range of wavelengths and power densities accessible with transfer-printed μ-ILEDs, together with their robust, high efficiency operation, enables their use as light source for various biomedical applications.[11,24,141,146,153] Recent work demonstrates multi-functional integrated systems for optogenetics,[24,141] an emerging field of neuroscience in which light exposure can stimulate or inhibit neural function. Here, InGaN μ-LEDs co-integrated with optical, thermal, and electrophysiology sensors and actuators in needle-like multilayer assemblies can be injected into the brain (**Figure 17**). The ultrasmall and thin geometries, low bending rigidities, and high degrees of mechanical flexibility enable a spatially precise, cellular-scale photon delivery vehicle, with reduced tissue damage and minimized inflammation compared to fiber optic alternatives.[24] The benefits in thermal management mentioned above, com-

bined with a pulse mode operation for the μ-ILEDs, allow operation with peak increases of temperature less than 0.10 °C for pulse frequencies less than 20 Hz. Fully wireless systems based on radiofrequency (RF) scavenging allow operation on freely moving, untethered animals.[11,24]

High yield microassembly of μ-ILEDs can also provide new opportunities for high pixel per inch (ppi) emissive display applications (**Figure 18**). The ultraminiaturized forms of μ-ILEDs (e.g., active area of ≈3 × 10 μm²) produce sufficient amounts of light for high luminance while occupying a small areal fraction of the pixels in the display, therefore allowing the panel arrays to accommodate a diverse range of additional microcomponents, including miniaturized integrated circuits for drivers, additional μ-ILEDs with different emission wavelengths, or other device components for extra functionality.
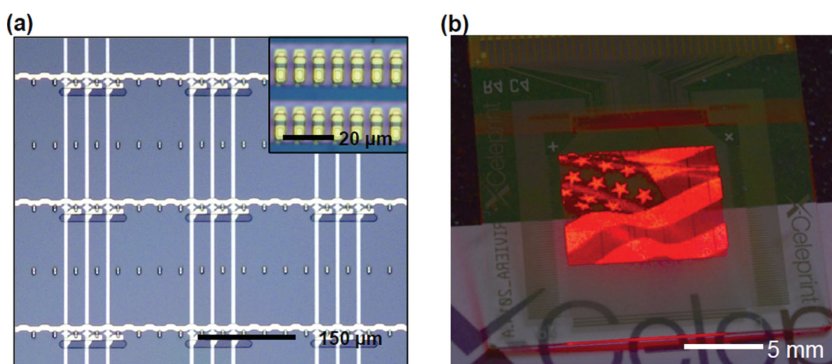
4.2. Organic LEDs

With organic or polymeric LEDs (OLEDs), transfer printing provides a means for patterning organic active layers into microscale pixels or constructing multilayered assemblies of different organic materials, where shadow mask deposition or conventional solution-based processes such as photolithography and spin-coating are not applicable due to the limited scalability and pixel resolution, incompatibility of the materials with the processing conditions (e.g., temperature, solvents, developers), or poor control of materials interfaces.[124,154–158] In one example, multilayers of organic active materials with aluminium cathodes deposited directly on a poly(urethane-acrylate) stamp pre-treated with a 20 nm-thick layer of fluorinated ethylene propylene (FEP) to reduce the adhesion can be transferred through successive printing operations to form red, green, and blue emitting layers for multi-color pixels in microscale layouts.[156]

In a related approach, bilayers of conjugated polymers formed by printing of individual layers with well-controlled organic-organic interfaces serve as active materials for organic LEDs.[124]

4.3. Quantum Dot LEDs

Inorganic colloidal semiconductor nanocrystals or quantum dots (QDs) based on CdSe, CdS, and ZnS represent promising alternatives to organic luminophores due to narrow emission bandwidths, high quantum efficiencies, a wide range of accessible bandgaps, and compatibility with solution processing.[159–167] Quantum dot based light emitting devices, or QLEDs, can be fabricated by placing a monolayer of quantum dots between electron

Figure 18. a) Optical image of sparse arrays of AlGaInP μ-ILEDs with an active area of ≈3 × 10 μm² printed on a glass substrate, interconnected in a passive matrix array. The inset shows dense arrays of μ-ILEDs formed on GaAs growth substrate. b) Passive matrix μ-ILED displays of 120 × 90 pixels, printed in a single stamping operation with a pixel size of ≈0.1 mm. Reproduced with permission. Copyright 2015, X-celeprint Inc.

and hole-transporting materials with appropriate energy band alignments.[161–165,167–169] Conventional solution-based deposition methods such as spin coating,[163,167,170,171] drop casting,[172,173] phase separation,[174] electrodeposition,[175–177] Langmuir–Schaefer transfer,[178,179] as well as inkjet printing[180] or electrohydrodynamic printing[181,182] suffer from constraints in film uniformity, interfacial smoothness, and/or materials compatibility between certain solvents and the active materials.[183,184] Furthermore, many of these methods have limitations in size-selective patterning of quantum dot domains with geometries essential for pixelated multicolor displays.[24,168,169,185–188]

Transfer printing solves many of these challenges. An early example involved patterning of uniform, densely-packed monolayers of QDs as the red-green-blue electroluminescent layers in QLEDs,[168,185] in which spin casting of QD solutions onto PDMS stamps constitutes the inking step. Chemically functionalizing the surfaces of the stamps with parylene-C prevents solvent uptake and associated swelling, improves the wetting of the QD suspension, and facilitates their transfer to the target substrate. Similar approaches work well in the formation of white QLEDs,[186] using mixed solutions of red, green, and blue CdSe/ZnS quantum dots (24%, 17%, and 59% by weight). Despite these successes, wet-inking processes require modifications to the PDMS stamps, with only limited control over the QD film morphology.

Methods that bypass such difficulties exploit dry transfer printing.[24,187–189] In one case, drop casting a solution of QDs onto a donor substrate followed by solvent annealing in an oversaturated atmosphere yields films with excellent long range order. Contact of a PDMS stamp allows selective removal of the QDs and enables their transfer to a target substrate in a completely dry process.[187] Sophisticated versions of this scheme allow realization of full-color QLED displays.[188] For this demonstration, chemically modifying the donor substrate with an octadecyltrichlorosilane self-assembled monolayer enhances the release of the QDs. Repetitive inking and printing processes in a step-and-repeat sequence yields patterned domains of QD on the receiving substrate. Controlled application of pressure during the printing step ensures that the QDs arrange into densely packed layers with a high degree of ordering both in-plane and out-of-plane.[189] The improved morphology and optimized interfaces lead to enhanced power efficiency and brightness compared with spin-cast QLEDs. Full-color, 4-inch active matrix QLED displays with resolution of 320 × 240 pixels follow from sequential transfer printing of multi-color QDs on substrates with hafnium-indium-zinc oxide (HIZO) thin film transistors (**Figure 19**a).[188] Further improvements are possible with the use of polyvinylalcohol (PVA) as a sacrificial layer to improve the yields in retrieving the QD monolayers.[190] Adhesive-less transfer by use temperature-modulated adhesion and applied shear force together with engineered surface energies of the 'receiver' QDs through the ligand exchange yields multilayer assemblies of QD monolayers. Such multilayer stacking
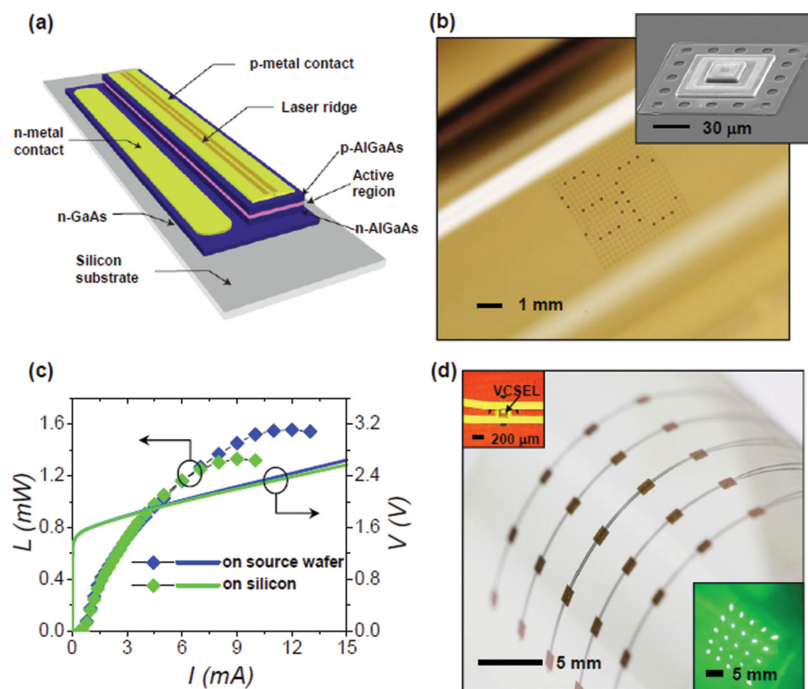

Figure 19. a) Photograph of a 4-inch full-color quantum dot display that uses a hafnium-indium-zinc oxide (HIZO) TFT backplane with a 320 × 240 pixel array. Reproduced with permission.[188] Copyright 2011, Nature Publishing Group. b) Electroluminescent device with a multistacked QD layer in a R(red)/G(green)/B(blue) sequence. Reproduced with permission.[190] Copyright 2013, Nature Publishing Group.

by transfer printing allows deterministic control over the energy-level alignment and energy transfer rate between constituent quantum dot layers, thereby leading to highly balanced white-light electroluminescence (Figure 19b).[190]

5. Lasers

Semiconductor diode lasers based on III–V epitaxial materials are widely used in optical communication systems, laser printers, barcode readers, CD/DVD players, as well as biomedical imaging devices and sensors.[191–195] Significant interest exists in the heterogeneous integration of such directional, coherent light emitters with dissimilar classes of materials and devices.[196–200] For example, light sources represent essential components for silicon-based integrated photonic circuits for on-chip communications.[199–201] Despite clever schemes for inducing light emission directly from the silicon itself[201–203] and for hybrid integration by heteroepitaxy,[204–208] and wafer bonding,[207,209,210] deficiencies in operating efficiencies, constraints associated with materials compatibility and complex processing requirements remain. In this context, transfer printing provides an attractive alternative that allows components (e.g., gain material or reflectors) of laser cavities or entire laser structures to be manipulated directly; it also creates design options that are unavailable to other approaches.[211–216]

In one example, epitaxial liftoff and transfer printing enables the integration of GaAs-based edge emitting lasers (EELs) onto silicon substrates for continuous wave (CW) operation (**Figure 20**a).[211] Lithographically defined microscale (≈400 × 100 μm²) 'coupons' of 5.7 μm-thick GaAs EEL epitaxial layers released by etching of sacrificial layer ($Al_{0.95}Ga_{0.05}As$) can be transferred to a silicon receiver substrate by van der Waals interactions alone, without using any adhesive layers, in which etching (ICP-RIE) forms the mirror facet required for the lasing. The resulting EEL on silicon exhibits single- and multi-transverse mode operation with total optical power of >60 mW, and laser characteristics such as threshold current, total slope efficiency, and small signal modulation bandwidth comparable to those of devices on the growth substrate. The etched facet approach also provides design freedom in the layout of the laser

Figure 20. a) Schematic illustration of GaAs-based edge emitting laser (EEL) transfer printed on a silicon substrate. Reproduced with permission.[211] Copyright 2012, Nature Publishing Group. b) Photograph of printed micro-VCSELs on a PET substrate with programmable spatial layouts (a logo of 'SC'). The inset shows a SEM image of a micro-VCSEL printed on a glass substrate. c) Representative current (I)–voltage (V) and optical output power (L)–current (I) data collected from 850 nm microVCSELs with an aperture of 7×7 μm^2, on the source GaAs wafer and after the printing on a silicon substrate using a thin (<1 μm) adhesive layer. Reproduced with permission.[214] Copyright 2014, John Wiley & Sons. (d) Photograph of 5×5 arrays of interconnected micro-VCSELs with an aperture area of 22×22 μm^2 on a thermally engineered flexible substrate, where micro-VCSELs are printed on square-shaped (1×1 mm^2) metal pads (Cr/Ag/Au: 10 nm/3000 nm/30 nm) patterned on a PET substrate. The inset shows the corresponding photograph of VCSEL illumination taken through an IR viewer and a magnified view of an individual micro-VCSEL with metal interconnects. Reproduced with permission.[230] Copyright 2015, John Wiley & Sons.

cavity including those, for example, with U-shaped retro-reflectors to double the effective cavity length and make better use of epitaxial materials.[211]
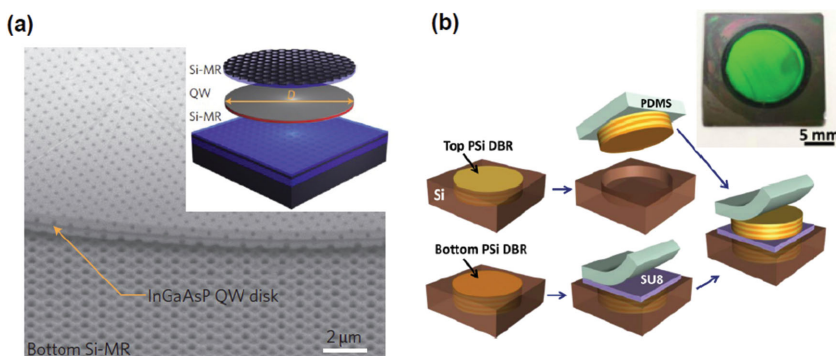
Vertical cavity surface emitting lasers (VCSELs) offer operational characteristics that complement those of EELs, such as surface-emitting beams with circular profiles, low beam divergence, reduced power consumption, as well as facile formation of arrayed layouts.[194,195,217,218] Like EELs, heterogeneous integration of VCSELs onto non-native substrates is valuable for a wide range of applications. As such, fabrication methods including flip-chip integration,[219,220] wafer-bonding,[221–223] fluidic assembly,[224,225] and epitaxial liftoff,[226,227] and applique[199,228,229] offer some value, but none provides practical pathways to manufacturing due to their high cost,[219,220] poor control over areal coverages,[224,225] tendency to degrade performance,[199,226,227] or limitations in substrate materials.[221,223] Here again, specialized epitaxial designs and liftoff approaches allow the use of transfer printing as an integration strategy.[214,230] Key aspects in the materials design include HF-resistant half-pair low index layers (e.g. Al$_{0.40}$Ga$_{0.60}$As), coplanar electrical contacts formed within the distributed Bragg reflectors

(DBRs), and double-mesa geometries for individual VCSEL, optimized for the protection of active layers during the undercut etching. The outcome enables defect-free release of ultrathin, microscale VCSELs (micro-VCSELs) from their growth wafers, in ways that are fully compatible with their deterministic assembly by transfer printing on virtually any type of non-native substrate in scalable, precisely controlled layouts (Figure 20b).[214] Micro-VCSELs with aperture areas of 7×7 μm^2 on silicon substrates exhibit IV and LV characteristics comparable to those on the source wafer, thereby confirming the absence of any degradation of the intrinsic materials properties of the DBRs or quantum wells (Figure 20c). Such printable forms of micro-VCSELs provide versatile choices in circuit- or system-level designs. Demonstrations include 10×10 arrays of individually addressable micro-VCSELs on thin (≈50 μm) PET substrates to form mechanically flexible, near-infrared laser displays, in which the electrical and optical characteristics of the devices remain invariant at bending radii of 2.5 mm, and up to 1000 cycles of bending due to the use of NMP layouts.[214] This scheme also allows integration of VCSELs with traditionally incompatible materials and devices to create unusual forms of function. For example, micro-VCSELs can serve as light sources on PET substrates co-integrated with silicon-based photodetectors to produce portable and miniaturized optoelectronic sensors for the detection of fluorescence or scattering signals as well as wearable physiological sensors for health monitoring. Thermally engineered composite assemblies of printed micro-VCSELs address core issues in thermal management, with particular relevance

to use of substrates with low thermal conductivities such as plastics.[230] Here, a thin metal layer incorporated between the devices and the PET substrate acts as a heat spreading medium to significantly reduce the effective thermal resistance of the system. The enhanced thermal characteristics can reach levels higher than those associated with the source wafer, while preserving critical benefits that follow from the use of mechanically flexible and optically transparent substrates (Figure 20d).[230]

Transfer printing can also be utilized for the assembly of discrete components of the laser cavities such as the reflectors and the gain materials to create new types of optically pumped lasers. The primary value of such approaches is in cases where monolithic growth and deposition are inherently limited or impossible due to mismatches in the materials properties and/or processing conditions.[212,216,231] Also, such assemblies avoid requirements in electrically connecting the gain medium and reflector, thereby creating choices in materials other than semiconductors for the laser cavity in optically pumped lasers. In one example, InGaAsP-based quantum well heterostructures combine with ultra-compact silicon-based photonic crystal reflectors to realize optically pumped inorganic lasers on silicon

www.MaterialsViews.com

ADVANCED
OPTICAL
MATERIALS
www.advopticalmat.de

REVIEW

Figure 21. a) SEM image of a complete MR-VCSEL, showing the InGaAsP quantum well disk sandwiched between top and bottom Si-MRs. The inset shows a schematic illustration of the multilayer printing process for the formation of an MR-VCSEL (top Si-MR/quantum well/bottom Si-MR). The diameter of the active layer is D. Reproduced with permission.[212] Copyright 2012, Nature Publishing Group. b) Schematic illustration of the process flow for the assembly of porous-silicon-based hybrid microcavities. The inset shows an optical image of completed structure. Reproduced with permission.[216] Copyright 2014, American Chemical Society.

(**Figure 21**a).[212] Transfer printing delivers epitaxially grown quantum well structures after their release from InP source substrates, onto SiO$_2$-coated silicon membrane reflectors (Si-MR) formed with square arrays of nanoholes fabricated by electron-beam lithography and reactive ion etching. An addition transfer printing step places Si-MRs on top, to form vertically stacked laser resonators. These thin (≈340 nm) membrane reflectors replace conventional thick DBRs found in VCSELs, to allow the lasers to be implemented directly on the silicon substrate with significantly reduced overall thickness (e.g., < ≈2 µm). Moreover, the ability to independently control the optical properties and spatial organization of individual reflectors allows multi-wavelength lasing operation on the same substrate.[212]

In another example, optically pumped laser structures based on porous-silicon DBRs can be realized by transfer printing (Figure 21b).[216] Porous silicon (PSi)-based DBRs produced on highly doped (0.01–0.03 Ωcm) (100) silicon wafers can be constructed with engineered stop-band position and high reflectance. Alternating stacks of high (≈2.4) and low (≈1.7) refractive index layers result from controlled electrochemical etching. Thin layers of gain media based on materials such as PbS nanocrystals (dispersed in SU-8) or layers of GaAs can be transfer printed on the bottom PSi DBR; another printing step forms the top DBR. The porosity of the silicon offers additional pathways to control the optical responses via infiltration of other materials. For example, the cavity resonances shift in expected ways by partially or completely introducing Al$_2$O$_3$ into PSi DBRs by atomic layer deposition, in a manner that does not broaden or diminish the strength of the resonant mode. Spatial modulation of the lasing behavior is possible by printing gain media (e.g., GaAs) onto various locations of DBRs that have gradient optical thicknesses and spatial variations in the cavity mode.[216]
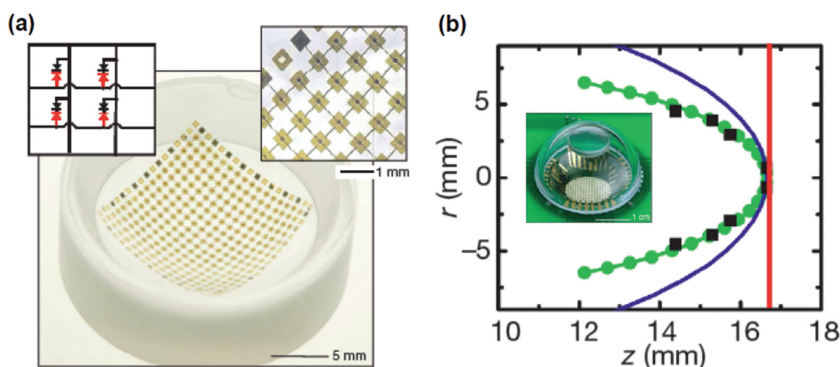
6. Photodetectors

Photodetectors represent one of the most widely utilized components in optoelectronics.[232,233] As with the other device classes discussed in this review, transfer printing offers versatile capabilities in integration, for both conventional and unconventional systems; examples of the latter include imaging arrays on plastic foils or rubber membranes for mechanically bendable modules for bio-integrated applications or bio-inspired designs.[13,87,135,234–243] Using processes similar to those described previously, photodetectors can be readily constructed from single-crystalline group IV (e.g., silicon and germanium)[214,235–238,240–243] and III–V (e.g., GaAs, InP)[13,234,239,244] semiconductors in forms compatible with transfer printing. As an example, eliminating the buried oxide layer from single-crystalline germanium-on-insulator (GOI) substrates after defining lateral p-i-n doping profiles in the top Ge by ion implantation yields 250 nm-thick germanium nanomembrane photodetectors that can be transfer printed onto PET substrates using a photocurable epoxy as an adhesive.[236] Related work shows that a 340 nm-thick, n-type silicon nanomembrane derived from silicon-on-insulator (SOI) substrates can be printed onto PET, where evaporation of p-type pentacene forms a heterojunction that can be used in flexible, semi-transparent photodetectors.[245]

Collections of photodiodes can be interconnected to create focal plane arrays for digital imagers[235,237,238,240,242,243]. Near-infrared (NIR) imaging systems can be formed on silicon substrates from printed arrays of photodetectors based on bilayers of undoped GaAs and n-type GaAs.[13] Deposition of Ti/Au forms metal–semiconductor–metal back-to-back diodes to enable NIR detection, while Schottky diodes made on the n-type GaAs layer serve to block reverse bias current and prevent cross-talk between pixels.[13] An even more compelling mode of integration involves assembly of photodetectors on hemispherically curved surfaces to create imaging devices with overall geometries similar to those commonly observed in biological systems.[235,237,238,240,242,243] Of historical interest in digital imaging are systems that exploit photodetectors on concave surfaces, in configurations similar to those of mammalian eyes, due to the ability of this geometry to match Petzval image surfaces associated with simple lenses.[246,247] Traditional optoelectronics technologies cannot reproduce this type of layout simply because all standard growth, deposition and fabrication processes exist only for use on planar surfaces of semiconductor wafers or glass substrates. Recent work demonstrates schemes based on transfer printing that can overcome such restrictions and realize high performance hemispherical imaging systems.[235]

The fabrication begins with transfer printing to form single-crystalline silicon photodiodes and blocking diodes using material derived from SOI wafers. Narrow metal interconnect lines encapsulated with thin polymer films in an NMP layout and configured to allow out-of-plane bending yields a layout that can be mechanically compressed to strains of several tens of percent without inducing fracture in the diodes. Geometric transformation of this originally planar array occurs by

ADVANCED
OPTICAL
MATERIALS
www.advopticalmat.de

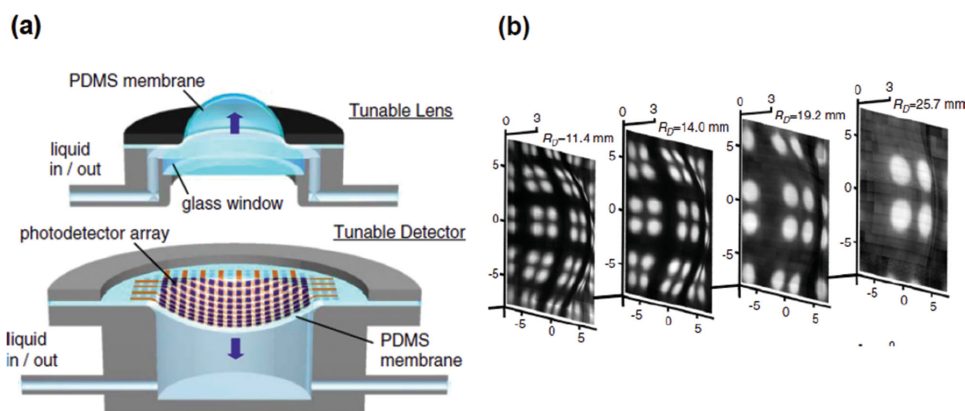Materials
Views
www.MaterialsViews.com

REVIEW

Figure 22. a) Photograph of an array of photodetectors (PDs) and blocking diodes (BDs) integrated on a hemispherical glass substrate (main frame), optical micrograph of a part of the array (upper right inset) and circuit diagram showing the BDs (black), PDs (red) and electrode crossovers (arcs) in a 2 × 2 section of the system (upper left inset). b) Ray tracing predictions of the curvature of the optimal focal surface (green circles, calculated focal points; green curve, parabolic fit), the detector surface of the hemispherical camera (blue curve), and a planar camera (red curve). The inset shows a photographic image of the electronic eye camera after integration with a transparent hemispherical cap with a simple, single-component imaging lens. Reproduced with permission.[235] Copyright 2008, Nature Publishing Group.

use of a thin elastomeric membrane cast into the shape of a hemispherical shell and then elastically deformed into a planar 'drumhead' by radial stretching. Transfer printing the entire interconnected array to the surface of the membrane and then releasing the radial tension allows the elastomer to return to its original shape, compressing and carrying the array with it (**Figure 22**a).[235] The compressive strains associated with this transformation cause the flexible interconnects to adopt out-of-plane arc-shaped structures.
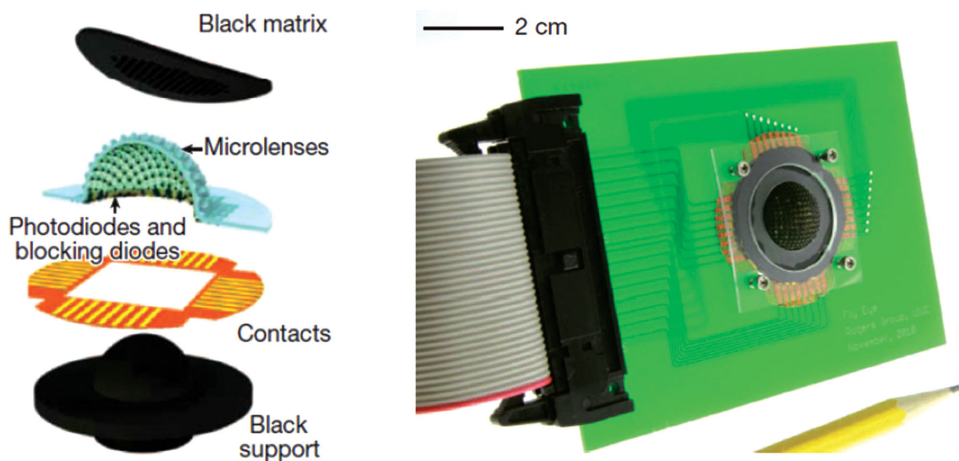
Forming a camera with this array involves bonding it to a solid hemispherical cavity machined into a glass substrate, integrating a plano-convex lens at the appropriate distance, and inserting the entire assembly into a hole in a printed circuit board that supports electrical connections to a separate data

acquisition system. Demonstrated "electronic eye" cameras of this type have approximately the same overall shape and size of the human eye.[235] As expected, the match between the curvature of the photodetector array and the Petzval surface improves the field of view and illumination uniformity, while reducing aberrations (Figure 22b). Many advanced versions of this type of system have been explored,[237,238,240,242,243] including recent examples by Sony in high resolution imagers.[248] The precise shape of the Petzval surface is better approximated by a paraboloid than a hemisphere; the same fabrication sequence, with appropriately designed elastomer membranes, can realize imagers with such shapes.[237] Multi-device tiles and extended non-coplanar interconnects can improve the fill factor and deformability.[238] The addition of hydraulic actuation schemes allows dynamic adjustment of the curvature, to enable use of imaging lenses with adjustable zoom capabilities (**Figure 23**).[240]

In the most sophisticated and most recent work in this area of bio-inspired design, extensions of the concepts described above enable digital cameras that mimic the architectures found in compound eyes of arthropods (**Figure 24**).[242] Here, an array of convex microlenses and cylindrical supporting posts molded on a stretchable base membrane bonds to a geometrically matched array of interconnected silicon photodiodes and blocking diodes, separately fabricated using transfer printing. Each photodiode lies at the focal plane of a corresponding microlens, to form artificial ommatidia.[242] Hydraulic actuation then deterministically transforms the planar layout of these bonded arrays into a full hemispherical shape, in a manner such that the interconnects and the base membrane accommodate nearly all of the strains. The resulting cameras provide two powerful characteristics that

Figure 23. a) Schematic illustration of an electronic eye camera with adjustable zoom, including the tunable lens (upper) and tunable detector (lower) modules. The lens consists of a fluid-filled gap between a thin PDMS membrane and a glass window, while the tunable detector consists of an array of interconnected silicon PDs and BDs mounted on a thin PDMS membrane. b) Images acquired by a complete camera system, collected at distances from the lens (z) of 16, 24, 38, and 55 mm with corresponding radii of curvature of the lens surface (R_L) of 4.9, 6.1, 7.3, and 11.5 mm. The radii of curvature (R_D) of the detector surface, set to match the computed Petzval surface shape, were 11.4, 14.0, 19.2, and 25.7 mm. Reproduced with permission.[240] Copyright 2011, The National Academy of Sciences.

Materials
Views
www.MaterialsViews.com

ADVANCED
OPTICAL
MATERIALS
www.advopticalmat.de

REVIEW

Figure 24. a) Exploded-view illustration of the components of a digital camera that takes the form of a hemispherical, apposition compound eye, including a perforated sheet of black silicone, hemispherical array of microlenses and PDs/BDs diodes, thin film contacts for external interconnects, and hemispherical supporting substrate of black silicone. b) Photograph of a completed camera mounted on a printed circuit board as an interface to external control electronics. Reproduced with permission.[242] Copyright 2013, Nature Publishing Group.

are unachievable by planar detector technologies (1) exceptionally wide-angle fields of view (as large as ≈160°) without off-axis aberrations and (2) nearly infinite depth of field due to the short focal lengths of the microlenses and the nature of image formation. These features enable simultaneous imaging of multiple objects at widely different angular positions and distances, with high acuity to motion.[242]

7. Conclusions

The results summarized here illustrate advances in the development of optoelectronic devices and their circuit/system-level implementation enabled by elastomeric-stamp-mediated transfer printing. They provide practical integration pathways to a broad spectrum of materials that can be co-integrated regardless of conditions for their growth, deposition, or patterning, and thereby maximize their performance and cost-effectiveness or impart novel hybrid functionalities and versatile capabilities not previously possible within established protocols. Some of the most appealing aspects include mechanically flexible and stretchable designs that allow high performance optoelectronic components derived from wafer-based inorganic semiconductors to be intimately integrated on curvilinear, deformable surfaces including skins and internal organs without compromising intrinsic materials properties and performance characteristics. The efforts covered in this review have yielded a wide range of results in device- and circuit-level deployment of such materials together with advanced fundamental understanding over many underlying scientific and engineering principles in materials science, device physics, surface chemistry, solid mechanics, and thermal transport. There exist many additional opportunities for basic and applied research in this field, for the development of novel processing techniques, device architectures, and system configurations, that will even further enhance application possibilities of both existing and emerging materials.

[1] X. Dai, B. M. Nguyen, Y. Hwang, C. Soci, S. A. Dayeh, *Adv. Funct. Mater.* **2014**, *24*, 4420.

[2] M. Lapisa, G. Stemme, F. Niklaus, *IEEE J. Sel. Top. Quant.* **2011**, *17*, 629.

[3] L. Xie, G. Yang, M. Mantysalo, L. L. Xu, F. Jonsson, L. R. Zheng, *IEEE J. Em. Sel. Top. C* **2012**, *2*, 672.

[4] S. W. Hwang, G. Park, H. Cheng, J. K. Song, S. K. Kang, L. Yin, J. H. Kim, F. G. Omenetto, Y. G. Huang, K. M. Lee, J. A. Rogers, *Adv. Mater.* **2014**, *26*, 1992.

[5] O. Moutanabbir, U. Goesele, in *Annual Review of Materials Research*, Vol. 40 (Eds: D. R. Clarke, M. Ruhle, F. Zok), **2010**, p. 469.

[6] A. J. Baca, J. H. Ahn, Y. G. Sun, M. A. Meitl, E. Menard, H. S. Kim, W. M. Choi, D. H. Kim, Y. Huang, J. A. Rogers, *Angew. Chem. Int. Ed.* **2008**, *47*, 5524.

[7] A. Carlson, A. M. Bowen, Y. G. Huang, R. G. Nuzzo, J. A. Rogers, *Adv. Mater.* **2012**, *24*, 5284.

[8] J. A. Rogers, M. G. Lagally, R. G. Nuzzo, *Nature* **2011**, *477*, 45.

[9] M. A. Meitl, Z. T. Zhu, V. Kumar, K. J. Lee, X. Feng, Y. Y. Huang, I. Adesida, R. G. Nuzzo, J. A. Rogers, *Nat. Mater.* **2006**, *5*, 33.

[10] D.-H. Kim, N. Lu, R. Ma, Y.-S. Kim, R.-H. Kim, S. Wang, J. Wu, S. M. Won, H. Tao, A. Islam, K. J. Yu, T.-i. Kim, R. Chowdhury, M. Ying, L. Xu, M. Li, H.-J. Chung, H. Keum, M. McCormick, P. Liu, Y.-W. Zhang, F. G. Omenetto, Y. Huang, T. Coleman, J. A. Rogers, *Science* **2011**, *333*, 838.

[11] R.-H. Kim, H. Tao, T.-i. Kim, Y. Zhang, S. Kim, B. Panilaitis, M. Yang, D.-H. Kim, Y. H. Jung, B. H. Kim, Y. Li, Y. Huang, F. G. Omenetto, J. A. Rogers, *Small* **2012**, *8*, 2812.

[12] J. Yoon, A. J. Baca, S.-I. Park, P. Elvikis, J. B. Geddes, L. Li, R. H. Kim, J. Xiao, S. Wang, T.-H. Kim, M. J. Motala, B. Y. Ahn, E. B. Duoss, J. A. Lewis, R. G. Nuzzo, P. M. Ferreira, Y. Huang, A. Rockett, J. A. Rogers, *Nat. Mater.* **2008**, *7*, 907.

[13] J. Yoon, S. Jo, I. S. Chun, I. Jung, H. S. Kim, M. Meitl, E. Menard, X. L. Li, J. J. Coleman, U. Paik, J. A. Rogers, *Nature* **2010**, *465*, 329.

[14] D. Qin, Y. N. Xia, G. M. Whitesides, *Nat. Protocols* **2010**, *5*, 491.

[15] Y. N. Xia, G. M. Whitesides, *Ann. Rev. Mater. Sci.* **1998**, *28*, 153.

[16] X. Feng, M. A. Meitl, A. M. Bowen, Y. Huang, R. G. Nuzzo, J. A. Rogers, *Langmuir* **2007**, *23*, 12555.

[17] A. Carlson, S. D. Wang, P. Elvikis, P. M. Ferreira, Y. G. Huang, J. A. Rogers, *Adv. Funct. Mater.* **2012**, *22*, 4476.

[18] S. Kim, J. A. Wu, A. Carlson, S. H. Jin, A. Kovalsky, P. Glass, Z. J. Liu, N. Ahmed, S. L. Elgan, W. Q. Chen, P. M. Ferreira, M. Sitti, Y. G. Huang, J. A. Rogers, *Proc. Natl. Acad. Sci. USA* **2010**, *107*, 17095.

[19] A. M. Al-okaily, J. A. Rogers, P. M. Ferreira, *J. Micro Nano-Manuf.* **2014**, *2*, 011002.

[20] R. Saeidpourazar, M. D. Sangid, J. A. Rogers, P. M. Ferreira, *J. Manuf. Processes* **2012**, *14*, 416.

[21] A. Carlson, H. J. Kim-Lee, J. Wu, P. Elvikis, H. Y. Cheng, A. Kovalsky, S. Elgan, Q. M. Yu, P. M. Ferreira, Y. G. Huang, K. T. Turner, J. A. Rogers, *Appl. Phys. Lett.* **2011**, *98*, 264104.

[22] H. Y. Cheng, J. Wu, Q. M. Yu, H. J. Kim-Lee, A. Carlson, K. T. Turner, K. C. Hwang, Y. G. Huang, J. A. Rogers, *Mech. Res. Commun.* **2012**, *43*, 46.

[23] Y.-L. Loo, R. L. Willett, K. W. Baldwin, J. A. Rogers, *J. Am. Chem. Soc.* **2002**, *124*, 7654.

[24] T. I. Kim, J. G. McCall, Y. H. Jung, X. Huang, E. R. Siuda, Y. H. Li, J. Z. Song, Y. M. Song, H. A. Pao, R. H. Kim, C. F. Lu, S. D. Lee, I. S. Song, G. Shin, R. Al-Hasani, S. Kim, M. P. Tan, Y. G. Huang, F. G. Omenetto, J. A. Rogers, M. R. Bruchas, *Science* **2013**, *340*, 211.

[25] Y. Yao, E. Brueckner, L. Li, R. Nuzzo, *Energy Environ. Sci.* **2013**, *6*, 3071.

[26] S. M. Won, H.-S. Kim, N. Lu, D.-G. Kim, C. Del Solar, T. Duenas, A. Ameen, J. A. Rogers, *IEEE Trans. Electron Devices* **2011**, *58*, 4074.

[27] S. I. Park, Y. J. Xiong, R. H. Kim, P. Elvikis, M. Meitl, D. H. Kim, J. Wu, J. Yoon, C. J. Yu, Z. J. Liu, Y. G. Huang, K. Hwang, P. Ferreira, X. L. Li, K. Choquette, J. A. Rogers, *Science* **2009**, *325*, 977.

[28] S. A. Vitale, H. Chae, H. H. Sawin, *J. Vac. Sci. Tech. A* **2000**, *18*, 2770.

[29] H. S. Kim, E. Brueckner, J. Z. Song, Y. H. Li, S. Kim, C. F. Lu, J. Sulkin, K. Choquette, Y. G. Huang, R. G. Nuzzo, J. A. Rogers, *Proc. Natl. Acad. Sci. USA* **2011**, *108*, 10072.

[30] S. Mack, M. A. Meitl, A. J. Baca, Z. T. Zhu, J. A. Rogers, *Appl. Phys. Lett.* **2006**, *88*, 213101.

[31] R.-H. Kim, D.-H. Kim, J. Xiao, B. H. Kim, S.-I. Park, B. Panilaitis, R. Ghaffari, J. Yao, M. Li, Z. Liu, V. Malyarchuk, D. G. Kim, A.-P. Le, R. G. Nuzzo, D. L. Kaplan, F. G. Omenetto, Y. Huang, Z. Kang, J. A. Rogers, *Nat. Mater.* **2010**, *9*, 929.

[32] A. Goetzberger, J. Luther, G. Willeke, *Sol. Energ. Mat. Sol. C* **2002**, *74*, 1.

[33] C. G. Granqvist, *Adv. Mater.* **2003**, *15*, 1789.

[34] T. Saga, *NPG Asia Mater.* **2010**, *2*, 96.

[35] M. A. Green, K. Emery, Y. Hishikawa, W. Warta, E. D. Dunlop, *Prog. Photovoltaics: Res. Appl.* **2015**, *23*, 1.

[36] S. Colle, S. L. De Abreu, R. Ruther, *Sol. Energy* **2001**, *70*, 131.

[37] D. M. Powell, M. T. Winkler, H. J. Choi, C. B. Simmons, D. B. Needleman, T. Buonassisi, *Energy Environ. Sci.* **2012**, *5*, 5874.

[38] C. H. Lee, D. R. Kim, X. Zheng, *ACS Nano* **2014**, *8*, 8746.

[39] T. Yonehara, K. Sakaguchi, N. Sato, *Appl. Phys. Lett.* **1994**, *64*, 2108.

[40] J. H. Petermann, D. Zielke, J. Schmidt, F. Haase, E. G. Rojas, R. Brendel, *Prog. Photovoltaics: Res. Appl.* **2012**, *20*, 1.

[41] J. N. Burghartz, W. Appel, H. D. Rempp, M. Zimmermann, *IEEE Trans. Electron Devices* **2009**, *56*, 321.

[42] M. Reuter, W. Brendle, O. Tobail, J. H. Werner, *Sol. Energ. Mat. Sol. C* **2009**, *93*, 704.

[43] S. W. Bedell, D. Shahrjerdi, B. Hekmatshoar, K. Fogel, P. A. Lauro, J. A. Ott, N. Sosa, D. Sadana, *IEEE J. Photovoltaics* **2012**, *2*, 141.

[44] F. Dross, J. Robbelein, B. Vandevelde, E. Van Kerschaver, I. Gordon, G. Beaucarne, J. Poortmans, *Appl. Phys. A* **2007**, *89*, 149.

[45] D. Shahrjerdi, S. W. Bedell, *Nano Lett.* **2013**, *13*, 315.

[46] A. J. Baca, K. J. Yu, J. Xiao, S. Wang, J. Yoon, J. H. Ryu, D. Stevenson, R. G. Nuzzo, A. A. Rockett, Y. Huang, J. A. Rogers, *Energy Environ. Sci.* **2010**, *3*, 208.

[47] D. Shir, J. Yoon, D. Chanda, J. H. Ryu, J. A. Rogers, *Nano Lett.* **2010**, *10*, 3041.

[48] J. Yoon, L. Li, A. V. Semichaevsky, J. H. Ryu, H. T. Johnson, R. G. Nuzzo, J. A. Rogers, *Nat. Commun.* **2011**, *2*, 343.

[49] K. J. Yu, L. Gao, J. S. Park, Y. R. Lee, C. J. Corcoran, R. G. Nuzzo, D. Chanda, J. A. Rogers, *Adv. Energy Mater.* **2013**, *3*, 1401.

[50] N. D. Bronstein, L. Li, L. Xu, Y. Yao, V. E. Ferry, A. P. Alivisatos, R. G. Nuzzo, *ACS Nano* **2014**, *8*, 44.

[51] S.-M. Lee, R. Biswas, W. Li, D. Kang, L. Chan, J. Yoon, *ACS Nano* **2014**, *8*, 10507.

[52] Z. Xu, Y. Yao, E. P. Brueckner, L. Li, J. Jiang, R. G. Nuzzo, G. L. Liu, *Nanotechnology* **2014**, 25.

[53] J. L. Cruz-Campa, M. Okandan, P. J. Resnick, P. Clews, T. Pluym, R. K. Grubbs, V. P. Gupta, D. Zubia, G. N. Nielson, *Sol. Energ. Mat. Sol. C* **2011**, *95*, 551.

[54] K. J. Weber, A. W. Blakers, M. J. Stocks, J. H. Babaei, V. A. Everett, A. J. Neuendorf, P. J. Verlinden, *IEEE Electron Device Lett.* **2004**, *25*, 37.

[55] E. Franklin, A. Blakers, V. Everett, *Prog. Photovoltaics* **2009**, *17*, 403.

[56] A. L. Lentine, G. N. Nielson, M. Okandan, J.-L. Cruz-Campa, A. Tauke-Pedretti, *IEEE J. Photovoltaics* **2014**, *4*, 1593.

[57] J. L. Cruz-Campa, G. N. Nielson, P. J. Resnick, C. A. Sanchez, P. J. Clews, M. Okandan, T. Friedmann, V. P. Gupta, *IEEE J. Photovoltaics* **2011**, *1*, 3.

[58] K. E. Bean, *IEEE Trans. Electron Devices* **1978**, *25*, 1185.

[59] H. Seidel, L. Csepregi, A. Heuberger, H. Baumgartel, *J. Electrochem. Soc.* **1990**, *137*, 3612.

[60] G. T. A. Kovacs, N. I. Maluf, K. E. Petersen, *Proc. IEEE* **1998**, *86*, 1536.

[61] G. N. Nielson, M. Okandan, J. L. Cruz-Campa, A. L. Lentine, W. C. Sweatt, B. H. Jared, P. J. Resnick, B. Kim, B. J. Anderson, V. P. Gupta, A. Tauke-Pedretti, J. G. Cederberg, T. Gu, M. W. Haney, S. M. Paap, C. A. Sanchez, C. Nordquist, M. P. Saavedra, M. Ballance, N. Janet, C. Alford, J. S. Nelson, *in* **2013**.

[62] D. H. Kim, J. H. Ahn, W. M. Choi, H. S. Kim, T. H. Kim, J. Z. Song, Y. G. Y. Huang, Z. J. Liu, C. Lu, J. A. Rogers, *Science* **2008**, *320*, 507.

[63] J. S. Batchelder, A. H. Zewail, T. Cole, *Appl. Optics* **1979**, *18*, 3090.

[64] M. G. Debije, P. P. C. Verbunt, *Adv. Energy Mater.* **2012**, *2*, 12.

[65] W. G. J. H. M. van Sark, K. W. J. Barnham, L. H. Slooff, A. J. Chatten, A. Buchtemann, A. Meyer, S. J. McCormack, R. Koole, D. J. Farrell, R. Bose, E. E. Bende, A. R. Burgers, T. Budel, J. Quilitz, M. Kennedy, T. Meyer, C. D. M. Donega, A. Meijerink, D. Vanmaekelbergh, *Optics Express* **2008**, *16*, 21773.

[66] J. Hu, C. R. Menyuk, *Adv. Optics Photonics* **2009**, *1*, 58.

[67] X. Sheng, L. Shen, T. Kim, L. F. Li, X. R. Wang, R. Dowdy, P. Froeter, K. Shigeta, X. L. Li, R. G. Nuzzo, N. C. Giebink, J. A. Rogers, *Adv. Energy Mater.* **2013**, *3*, 991.

[68] R. A. Sinton, Y. Kwark, J. Y. Gan, R. M. Swanson, *IEEE Electron Device Lett.* **1986**, *7*, 567.

[69] S. B. Mallick, M. Agrawal, P. Peumans, *Optics Express* **2010**, *18*, 5691.

[70] D. M. Callahan, J. N. Munday, H. A. Atwater, *Nano Lett.* **2012**, *12*, 214.

[71] P. Spinelli, V. E. Ferry, J. van de Groep, M. van Lare, M. A. Verschuuren, R. E. I. Schropp, H. A. Atwater, A. Polman, *J. Optics* **2012**, *14*, 024002.

[72] P. Papet, O. Nichiporuk, A. Kaminski, Y. Rozier, J. Kraiem, J. F. Lelievre, A. Chaumartin, A. Fave, M. Lemiti, *Sol. Energ. Mat. Sol. C* **2006**, *90*, 2319.

[73] D. Iencinella, E. Centurioni, R. Rizzoli, F. Zignani, *Sol. Energ. Mat. Sol. C* **2005**, *87*, 725.

[74] M. Yu, Y. Z. Long, B. Sun, Z. Y. Fan, *Nanoscale* **2012**, *4*, 2783.

[75] M. L. Brongersma, Y. Cui, S. Fan, *Nat Mater* **2014**, *13*, 451.

[76] S. Jeong, M. D. McGehee, Y. Cui, *Nat. Commun.* **2013**, *4*, 2950.

[77] S. Mokkapati, K. R. Catchpole, *J. Appl. Phys.* **2012**, *112*, 101101.

[78] J. Y. Kwon, D. H. Lee, M. Chitambar, S. Maldonado, A. Tuteja, A. Boukai, *Nano Lett.* **2012**, *12*, 5143.

[79] Z. Huang, N. Geyer, P. Werner, J. de Boor, U. Goesele, *Adv. Mater.* **2011**, *23*, 285.

[80] M. Kroll, M. Otto, T. Kaesebier, K. Fuechsel, R. Wehrspohn, E.-B. Kley, A. Tuennermann, T. Pertsch, *Proc. SPIE* **2012**, *8438*, 843817.

[81] J. Oh, H.-C. Yuan, H. M. Branz, *Nat. Nanotechnol.* **2012**, *7*, 743.

[82] M. Yamaguchi, T. Takamoto, K. Araki, N. Ekins-Daukes, *Sol. Energy* **2005**, *79*, 78.

[83] F. Dimroth, *Phys. Stat. Solidi C* **2006**, *3*, 373.

[84] M. Woodhouse, A. Goodrich, *NREL Report* **2014**, *PR-6A20-60126*, 92.

[85] J. Lee, J. A. Wu, M. X. Shi, J. Yoon, S. I. Park, M. Li, Z. J. Liu, Y. G. Huang, J. A. Rogers, *Adv. Mater.* **2011**, *23*, 986.

[86] J. Lee, J. Wu, J. H. Ryu, Z. J. Liu, M. Meitl, Y. W. Zhang, Y. G. Huang, J. A. Rogers, *Small* **2012**, *8*, 1851.

[87] D. S. Kang, S. Arab, S. B. Cronin, X. L. Li, J. A. Rogers, J. Yoon, *Appl. Phys. Lett.* **2013**, *102*, 253902.

[88] W. Choi, C. Z. Kim, C. S. Kim, W. Heo, T. Joo, S. Y. Ryu, H. Kim, H. Kim, H. K. Kang, S. Jo, *Adv. Energy Mater.* **2014**, 4, 1400589.

[89] X. Sheng, C. A. Bower, S. Bonafede, J. W. Wilson, B. Fisher, M. Meitl, H. Yuen, S. D. Wang, L. Shen, A. R. Banks, C. J. Corcoran, R. G. Nuzzo, S. Burroughs, J. A. Rogers, *Nat. Mater.* **2014**, *13*, 593.

[90] X. Sheng, C. J. Corcoran, J. He, L. Shen, S. Kim, J. Park, R. G. Nuzzo, J. A. Rogers, *Phys. Chem. Chem. Phys.* **2013**, *15*, 20434.

[91] J. S. Price, X. Sheng, B. M. Meulblok, J. A. Rogers, N. C. Giebink, *Nat. Commun.* **2015**, *6*, 6223.

[92] X. Sheng, M. H. Yun, C. Zhang, A. M. Al-Okaily, M. Masouraki, L. Shen, S. D. Wang, W. L. Wilson, J. Y. Kim, P. Ferreira, X. L. Li, E. Yablonovitch, J. A. Rogers, *Adv. Energy Mater.* **2015**.

[93] B. Furman, E. Menard, A. Gray, M. Meitl, S. Bonafede, D. Kneeburg, K. Ghosal, R. Bukovnik, W. Wagner, J. Gabriel, S. Seel, S. Burroughs, in *35th IEEE Photovoltaic Specialists Conference,* **2010**.

[94] M. Konagai, M. Sugimoto, K. Takahashi, *J. Crystal Growth* **1978**, *45*, 277.

[95] E. Yablonovitch, T. Gmitter, J. P. Harbison, R. Bhat, *Appl. Phys. Lett.* **1987**, *51*, 2222.

[96] E. Yablonovitch, D. M. Hwang, T. J. Gmitter, L. T. Florez, J. P. Harbison, *Appl. Phys. Lett.* **1990**, *56*, 2419.

[97] C. Camperiginestet, M. Hargis, N. Jokerst, M. Allen, *IEEE Phot. Technol. Lett.* **1991**, *3*, 1123.

[98] X. Y. Lee, A. K. Verma, C. Q. Wu, M. Goertemiller, E. Yablonovitch, J. Eldredge, D. Lillington, in 25th IEEE Photovoltaic Specialists Conference, **1996**.

[99] Y. Yazawa, J. Minemura, K. Tamura, S. Watahiki, T. Kitatani, T. Warabisako, *Sol. Energ. Mat. Sol. C* **1998**, *50*, 163.

[100] R. Tatavarti, G. Hillier, A. Dzankovic, G. Martin, F. Tuminello, R. Navaratnarajah, G. Du, D. P. Vu, N. Pan, in *33rd IEEE Photovoltaic Specialists Conference,* **2008**.

[101] R. Tatavarti, G. Hillier, G. Martin, A. Wibowo, R. Navaratnarajah, F. Tuminello, D. Hertkorn, M. Disabb, C. Youtsey, D. McCallum, N. Pan, in *34th IEEE Photovoltaic Specialists Conference,* **2009**.

[102] R. Tatavarti, A. Wibowo, G. Martin, F. Tuminello, C. Youtsey, G. Hillier, N. Pan, M. W. Wanlass, M. Romero, in *35th IEEE Photovoltaic Specialists Conference*, **2010**.

[103] C. W. Cheng, K. T. Shiu, N. Li, S. J. Han, L. Shi, D. K. Sadana, *Nat. Commun.* **2013**, *4*, 1577.

[104] B. M. Kayes, L. Zhang, I. K. Ding, G. S. Higashi, *IEEE J. Photovoltaics* **2014**, *4*, 729.

[105] B. M. Kayes, N. Hui, R. Twist, S. G. Spruytte, F. Reinhardt, I. C. Kizilyalli, G. S. Higashi, in *37th IEEE Photovoltaic Specialists Conference,* **2011**.

[106] W. Shockley, H. J. Queisser, *J. Appl. Phys.* **1961**, *32*, 510.

[107] T. Trupke, M. A. Green, P. Wurfel, *J. Appl. Phys.* **2002**, *92*, 1668.

[108] R. M. France, J. F. Geisz, I. Garcia, M. A. Steiner, W. E. McMahon, D. J. Friedman, T. E. Moriarty, C. Osterwald, J. S. Ward, A. Duda, M. Young, W. J. Olavarria, *IEEE J. Photovoltaics* **2015**, *5*, 432.

[109] W. Guter, J. Schoene, S. P. Philipps, M. Steiner, G. Siefer, A. Wekkeli, E. Welser, E. Oliva, A. W. Bett, F. Dimroth, *Appl. Phys. Lett.* **2009**, *94*, 223504.

[110] M. Yamaguchi, *Sol. Energ. Mat. Sol. C* **2003**, *75*, 261.

[111] A. Moto, S. Tanaka, T. Tanabe, S. Takagishi, *Sol. Energ. Mat. Sol. C* **2001**, *66*, 585.

[112] L. D. Partain, M. S. Kuryla, R. E. Weiss, R. A. Ransom, P. S. McLeod, L. M. Fraas, J. A. Cape, *J. Appl. Phys.* **1987**, *62*, 3010.

[113] H. Matsubara, T. Tanabe, A. Moto, Y. Mine, S. Takagishi, *Sol. Energ. Mat. Sol. C* **1998**, *50*, 177.

[114] K. Zahraman, J. C. Guillaume, G. Nataf, B. Beaumont, M. Leroux, P. Gibart, *Jap. J. Appl. Phys. 1* **1994**, *33*, 5807.

[115] K. Ghosal, D. Lilly, J. Gabriel, S. Seel, E. Menard, S. Burroughs, R. Daniel, S. Lowe, C. Kudija, *8th Int. Conf. Concentrating Photovoltaic Systems* **2012**, *1477*, 327.

[116] K. Ghosal, S. Burroughs, K. Heuser, D. Setz, E. Garralaga-Rojas, *Prog. Photovoltaics* **2013**, *21*, 1370.

[117] R. H. Friend, R. W. Gymer, A. B. Holmes, J. H. Burroughes, R. N. Marks, C. Taliani, D. D. C. Bradley, D. A. Dos Santos, J. L. Bredas, M. Logdlund, W. R. Salaneck, *Nature* **1999**, *397*, 121.

[118] G. Li, V. Shrotriya, J. S. Huang, Y. Yao, T. Moriarty, K. Emery, Y. Yang, *Nat. Mater.* **2005**, *4*, 864.

[119] Y. Sun, G. C. Welch, W. L. Leong, C. J. Takacs, G. C. Bazan, A. J. Heeger, *Nat. Mater.* **2012**, *11*, 44.

[120] S. R. Forrest, *Nature* **2004**, *428*, 911.

[121] P. T. Hammond, *Adv. Mater.* **2004**, *16*, 1271.

[122] E. Moons, *J. Phys. Condens. Matter* **2002**, *14*, 12235.

[123] A. J. Heeger, *Chem. Soc. Rev.* **2010**, *39*, 2354.

[124] K.-H. Yim, Z. Zheng, Z. Liang, R. H. Friend, W. T. S. Huck, J.-S. Kim, *Adv. Funct. Mater.* **2008**, *18*, 1012.

[125] L. Chen, P. Degenaar, D. D. C. Bradley, *Adv. Mater.* **2008**, *20*, 1679.

[126] J.-H. Huang, Z.-Y. Ho, T.-H. Kuo, D. Kekuda, C.-W. Chu, K.-C. Ho, *J. Mater. Chem.* **2009**, *19*, 4077.

[127] Y. J. Cho, J. Y. Lee, S. R. Forrest, *Appl. Phys. Lett.* **2013**, 103, 193301.

[128] D. H. Wang, D. G. Choi, K.-J. Lee, O. O. Park, J. H. Park, *Org. Electron.* **2010**, *11*, 599.

[129] F.-C. Chen, M.-K. Chuang, S.-C. Chien, J.-H. Fang, C.-W. Chu, *J. Mater. Chem.* **2011**, *21*, 11378.

[130] X. Wang, T. Ishwara, W. Gong, M. Campoy-Quiles, J. Nelson, D. D. C. Bradley, *Adv. Funct. Mater.* **2012**, *22*, 1454.

[131] D.-G. Choi, K.-J. Lee, J.-H. Jeong, D. H. Wang, O. O. Park, J. H. Park, *Sol. Energ. Mat. Sol. C* **2013**, *109*, 1.

[132] D. A. Gaul, W. S. Rees, *Adv. Mater.* **2000**, *12*, 935.

[133] S. Nakamura, G. Fasol, *The Blue Laser Diode: GaN Based Light Emitters and Lasers*, Springer-Verlag, Berlin/Heidelberg, Germany **1997**.

[134] R.-H. Kim, M.-H. Bae, D. G. Kim, H. Cheng, B. H. Kim, D.-H. Kim, M. Li, J. Wu, F. Du, H.-S. Kim, S. Kim, D. Estrada, S. W. Hong, Y. Huang, E. Pop, J. A. Rogers, *Nano Lett.* **2011**, *11*, 3881.

[135] R.-H. Kim, S. Kim, Y. M. Song, H. Jeong, T.-i. Kim, J. Lee, X. Li, K. D. Choquette, J. A. Rogers, *Small* **2012**, *8*, 3123.

[136] T.-i. Kim, S. Hyun Lee, Y. Li, Y. Shi, G. Shin, S. Dan Lee, Y. Huang, J. A. Rogers, J. Su Yu, *Appl. Phys. Lett.* **2014**, 104, 051901.

[137] S.-I. Park, A.-P. Le, J. Wu, Y. Huang, X. Li, J. A. Rogers, *Adv. Mater.* **2010**, *22*, 3062.

[138] D.-H. Kim, N. Lu, R. Ghaffari, Y.-S. Kim, S. P. Lee, L. Xu, J. Wu, R.-H. Kim, J. Song, Z. Liu, J. Viventi, B. de Graff, B. Elolampi, M. Mansour, M. J. Slepian, S. Hwang, J. D. Moss, S.-M. Won, Y. Huang, B. Litt, J. A. Rogers, *Nat. Mater.* **2011**, *10*, 316.

[139] E. F. Schubert, J. K. Kim, *Science* **2005**, *308*, 1274.

[140] Y. Narukawa, M. Ichikawa, D. Sanga, M. Sano, T. Mukai, *J. Phys. D-Appl. Phys.* **2010**, 43, 354002.

[141] J. G. McCall, T.-i. Kim, G. Shin, X. Huang, Y. H. Jung, R. Al-Hasani, F. G. Omenetto, M. R. Bruchas, J. A. Rogers, *Nat. Protocols* **2013**, *8*, 2413.

[142] Y. Jung, X. Wang, J. Kim, S. Hyun Kim, F. Ren, S. J. Pearton, J. Kim, *Appl. Phys. Lett.* **2012**, *100*, 231113.

[143] W.-S. Choi, H. J. Park, S.-H. Park, T. Jeong, *IEEE Phot. Technol. Lett.* **2014**, *26*, 2115.

[144] S. Guha, N. A. Bojarczuk, *Appl. Phys. Lett.* **1998**, *72*, 415.

[145] A. J. Trindade, B. Guilhabert, D. Massoubre, D. Zhu, N. Laurand, E. Gu, I. M. Watson, C. J. Humphreys, M. D. Dawson, *Appl. Phys. Lett.* **2013**, 103, 253302.

[146] S. Y. Lee, K. I. Park, C. Huh, M. Koo, H. G. Yoo, S. Kim, C. S. Ah, G. Y. Sung, K. J. Lee, *Nano Energy* **2012**, *1*, 145.

[147] S. H. Park, G. Yuan, D. T. Chen, K. L. Xiong, J. Song, B. Leung, J. Han, *Nano Lett.* **2014**, *14*, 4293.

[148] T. Makimoto, K. Kumakura, Y. Kobayashi, T. Akasaka, H. Yamamoto, *Appl. Phys. Express* **2012**, *5*, 072102.

[149] Y. Kobayashi, K. Kumakura, T. Akasaka, T. Makimoto, *Nature* **2012**, *484*, 223.

[150] C. F. Lu, Y. H. Li, J. Z. Song, H. S. Kim, E. Brueckner, B. Fang, K. C. Hwang, Y. G. Huang, R. G. Nuzzo, J. A. Rogers, *Proc. R. Soc. A-Math. Phys. Eng. Sci.* **2012**, *468*, 3215.

[151] T.-i. Kim, Y. H. Jung, J. Song, D. Kim, Y. Li, H.-s. Kim, I.-S. Song, J. J. Wierer, H. A. Pao, Y. Huang, J. A. Rogers, *Small* **2012**, *8*, 1643.

[152] Y. H. Li, Y. Shi, J. Z. Song, C. F. Lu, T. I. Kim, J. A. Rogers, Y. G. Huang, *J. Appl. Phys.* **2013**, 113, 144505.

[153] C. Gossler, C. Bierbrauer, R. Moser, M. Kunzer, K. Holc, W. Pletschen, K. Kohler, J. Wagner, M. Schwaerzle, P. Ruther, O. Paul, J. Neef, D. Keppeler, G. Hoch, T. Moser, U. T. Schwarz, *J. Phys. D* **2014**, 47, 205401.

[154] M. L. Chabinyc, A. Salleo, Y. Wu, P. Liu, B. S. Ong, M. Heeney, I. McCulloch, *J. Am. Chem. Soc.* **2004**, *126*, 13928.

[155] C. Kim, Y. Cao, W. O. Soboyejo, S. R. Forrest, *J. Appl. Phys.* **2005**, *97*, 113512.

[156] J.-H. Choi, K.-H. Kim, S.-J. Choi, H. H. Lee, *Nanotechnology* **2006**, *17*, 2246.

[157] J. Choi, D. Kim, P. J. Yoo, H. H. Lee, *Adv. Mater.* **2005**, *17*, 166.

[158] H. Z. Jin, J. C. Sturm, *J. Soc. Inf. Disp.* **2010**, *18*, 141.

[159] D. J. Norris, A. L. Efros, M. Rosen, M. G. Bawendi, *Phys. Rev. B* **1996**, *53*, 16347.

[160] N. Tessler, V. Medvedev, M. Kazes, S. H. Kan, U. Banin, *Science* **2002**, *295*, 1506.

[161] V. L. Colvin, M. C. Schlamp, A. P. Alivisatos, *Nature* **1994**, *370*, 354.

[162] S. Coe, W. K. Woo, M. Bawendi, V. Bulovic, *Nature* **2002**, *420*, 800.

[163] J. L. Zhao, J. A. Bardecker, A. M. Munro, M. S. Liu, Y. H. Niu, I. K. Ding, J. D. Luo, B. Q. Chen, A. K. Y. Jen, D. S. Ginger, *Nano Lett.* **2006**, *6*, 463.

[164] J. M. Caruge, J. E. Halpert, V. Wood, V. Bulovic, M. G. Bawendi, *Nat. Photonics* **2008**, *2*, 247.

[165] P. O. Anikeeva, J. E. Halpert, M. G. Bawendi, V. Bulovic, *Nano Lett.* **2009**, *9*, 2532.

[166] J. S. Steckel, P. Snee, S. Coe-Sullivan, J. R. Zimmer, J. E. Halpert, P. Anikeeva, L. A. Kim, V. Bulovic, M. G. Bawendi, *Angew. Chem.-Int. Ed.* **2006**, *45*, 5796.

[167] K. S. Cho, E. K. Lee, W. J. Joo, E. Jang, T. H. Kim, S. J. Lee, S. J. Kwon, J. Y. Han, B. K. Kim, B. L. Choi, J. M. Kim, *Nat. Photonics* **2009**, *3*, 341.

[168] V. Wood, M. J. Panzer, J. E. Halpert, J. M. Caruge, M. G. Bawendi, V. Bulovic, *ACS Nano* **2009**, *3*, 3581.

[169] V. Wood, M. J. Panzer, J. M. Caruge, J. E. Halpert, M. G. Bawendi, V. Bulovic, *Nano Lett.* **2010**, *10*, 24.

[170] Q. Sun, Y. A. Wang, L. S. Li, D. Y. Wang, T. Zhu, J. Xu, C. H. Yang, Y. F. Li, *Nat. Photonics* **2007**, *1*, 717.

[171] S. Chaudhary, M. Ozkan, W. C. W. Chan, *Appl. Phys. Lett.* **2004**, *84*, 2925.

[172] S. Keuleyan, E. Lhuillier, V. Brajuskovic, P. Guyot-Sionnest, *Nat. Photonics* **2011**, *5*, 489.

[173] D. D. Vaughn, R. J. Patel, M. A. Hickner, R. E. Schaak, *J. Am. Chem. Soc.* **2010**, *132*, 15170.

[174] S. Coe-Sullivan, J. S. Steckel, W. K. Woo, M. G. Bawendi, V. Bulovic, *Adv. Funct. Mater.* **2005**, *15*, 1117.

[175] P. Brown, P. V. Kamat, *J. Am. Chem. Soc.* **2008**, *130*, 8890.

[176] X. Y. Yu, J. Y. Liao, K. Q. Qiu, D. B. Kuang, C. Y. Su, *ACS Nano* **2011**, *5*, 9494.

[177] X. N. Wang, H. J. Zhu, Y. M. Xu, H. Wang, Y. Tao, S. Hark, X. D. Xiao, Q. A. Li, *ACS Nano* **2010**, *4*, 3302.

[178] G. M. Lowman, S. L. Nelson, S. A. Graves, G. F. Strouse, S. K. Buratto, *Langmuir* **2004**, *20*, 2057.

[179] K. Lambert, R. K. Capek, M. I. Bodnarchuk, M. V. Kovalenko, D. Van Thourhout, W. Heiss, Z. Hens, *Langmuir* **2010**, *26*, 7732.

[180] V. Wood, M. J. Panzer, J. Chen, M. S. Bradley, J. E. Halpert, M. G. Bawendi, V. Bulović, *Adv. Mater.* **2009**, *21*, 2151.

[181] B. H. Kim, M. S. Onses, J. B. Lim, S. Nam, N. Oh, H. Kim, K. J. Yu, J. W. Lee, J.-H. Kim, S.-K. Kang, C. H. Lee, J. Lee, J. H. Shin, N. H. Kim, C. Leal, M. Shim, J. A. Rogers, *Nano Lett.* **2015**, *15*, 969.

[182] S. J. P. Kress, P. Richner, S. V. Jayanti, P. Galliker, D. K. Kim, D. Poulikakos, D. J. Norris, *Nano Lett.* **2014**, *14*, 5827.

[183] V. Wood, M. J. Panzer, J. L. Chen, M. S. Bradley, J. E. Halpert, M. C. Bawendi, V. Bulovic, *Adv. Mater.* **2009**, *21*, 2151.

[184] T. Zhu, K. Shanmugasundaram, S. C. Price, J. Ruzyllo, F. Zhang, J. Xu, S. E. Mohney, Q. Zhang, A. Y. Wang, *Appl. Phys. Lett.* **2008**, *92*, 023111.

[185] L. Kim, P. O. Anikeeva, S. A. Coe-Sullivan, J. S. Steckel, M. G. Bawendi, V. Bulovic, *Nano Lett.* **2008**, *8*, 4513.

[186] A. Rizzo, M. Mazzeo, M. Biasiucci, R. Cingolani, G. Gigli, *Small* **2008**, *4*, 2143.

[187] A. Rizzo, M. Mazzeo, M. Palumbo, G. Lerario, S. D'Amone, R. Cingolani, G. Gigli, *Adv. Mater.* **2008**, *20*, 1886.

[188] T. H. Kim, K. S. Cho, E. K. Lee, S. J. Lee, J. Chae, J. W. Kim, D. H. Kim, J. Y. Kwon, G. Amaratunga, S. Y. Lee, B. L. Choi, Y. Kuk, J. M. Kim, K. Kim, *Nat. Photonics* **2011**, *5*, 176.

[189] S. Lee, D. Yoon, D. Choi, T. H. Kim, *Nanotechnology* **2013**, 24, 025702.

[190] T. H. Kim, D. Y. Chung, J. Ku, I. Song, S. Sul, D. H. Kim, K. S. Cho, B. L. Choi, J. M. Kim, S. Hwang, K. Kim, *Nat. Commun.* **2013**, *4*, 2637.

[191] H. Morkoc, S. Strite, G. B. Gao, M. E. Lin, B. Sverdlov, M. Burns, *J. Appl. Phys.* **1994**, *76*, 1363.

[192] P. Werle, *Spectrochim Acta A* **1998**, *54*, 197.

[193] J. S. Harris, *Semicond. Sci. Tech.* **2002**, *17*, 880.

www.MaterialsViews.com

ADVANCED
OPTICAL
MATERIALS
www.advopticalmat.de

REVIEW

[194] J. S. Harris, T. O'Sullivan, T. Sarmiento, M. M. Lee, S. Vo, *Semicond. Sci. Tech.* **2011**, 26, 014010.

[195] K. Iga, *Proc. IEEE* **2013**, *101*, 2229.

[196] D. L. Mathine, D. R. Allee, R. Droopad, G. N. Maracas, *Appl. Phys. Lett.* **1996**, *69*, 463.

[197] R. Pu, E. M. Hayes, C. W. Wilmsen, K. D. Choquette, H. Q. Hou, K. M. Geib, *J. Opt. A* **1999**, *1*, 324.

[198] H. T. Hattori, C. Seassal, E. Touraille, P. Rojo-Rmeo, X. Letartre, G. Hollinger, P. Viktorovitch, L. Di Cioccio, M. Zussy, L. El Melhaoui, J. M. Fedeli, *IEEE Phot. Technol. Lett.* **2006**, *18*, 223.

[199] D. L. Mathine, *IEEE J. Sel. Top. Quant.* **1997**, *3*, 952.

[200] S. M. Zakharov, V. B. Fedorov, V. V. Tsvetkov, *Quantum Electron* **1999**, *29*, 745.

[201] Y. Takahashi, Y. Inui, M. Chihara, T. Asano, R. Terawaki, S. Noda, *Nature* **2013**, *498*, 470.

[202] R. Claps, D. Dimitropoulos, Y. Han, B. Jalali, *Opt. Express* **2002**, *10*, 1305.

[203] O. Boyraz, B. Jalali, *Opt. Express* **2004**, *12*, 5269.

[204] Z. Mi, R. Bhattacharya, J. Yang, K. P. Pipe, *Electron Lett.* **2005**, *41*, 742.

[205] G. Balakrishnan, A. Jallipalli, P. Rotella, S. H. Huang, A. Khoshakhlagh, A. Amtout, S. Krishna, L. R. Dawson, D. L. Huffaker, *IEEE J. Sel. Top. Quant.* **2006**, *12*, 1636.

[206] R. Chen, T. T. D. Tran, K. W. Ng, W. S. Ko, L. C. Chuang, F. G. Sedgwick, C. Chang-Hasnain, *Nat. Photonics* **2011**, *5*, 170.

[207] D. Liang, J. E. Bowers, *Nat. Photonics* **2010**, *4*, 511.

[208] A. Lee, H. Y. Liu, A. Seeds, *Semicond. Sci. Tech.* **2013**, *28*, 015027.

[209] G. Roelkens, L. Liu, D. Liang, R. Jones, A. Fang, B. Koch, J. Bowers, *Laser Phot. Rev.* **2010**, *4*, 751.

[210] K. Tanabe, K. Watanabe, Y. Arakawa, *Sci. Rep.* **2012**, *2*, 349.

[211] J. Justice, C. Bower, M. Meitl, M. B. Mooney, M. A. Gubbins, B. Corbett, *Nat. Photonics* **2012**, *6*, 610.

[212] H. J. Yang, D. Y. Zhao, S. Chuwongin, J. H. Seo, W. Q. Yang, Y. C. Shuai, J. Berggren, M. Hammar, Z. Q. Ma, W. D. Zhou, *Nat. Photonics* **2012**, *6*, 615.

[213] B. Corbett, C. Bower, A. Fecioru, M. Mooney, M. Gubbins, J. Justice, *Semicond. Sci. Tech.* **2013**, *28*, 094001.

[214] D. Kang, S. M. Lee, Z. W. Li, A. Seyedi, J. O'Brien, J. L. Xiao, J. Yoon, *Adv. Opt. Mater.* **2014**, *2*, 373.

[215] I. Karnadi, J. Son, J.-Y. Kim, H. Jang, S. Lee, K. S. Kim, B. Min, Y.-H. Lee, *Optics Express* **2014**, *22*, 12115.

[216] H. Ning, N. A. Krueger, X. Sheng, H. Keurn, C. Zhang, K. D. Choquette, X. L. Li, S. Kim, J. A. Rogers, P. V. Braun, *ACS Photonics* **2014**, *1*, 1144.

[217] K. D. Choquette, H. Q. Hou, *Proc. IEEE* **1997**, *85*, 1730.

[218] K. Iga, *Jpn. J. Appl. Phys.* **2008**, *47*, 1.

[219] R. Safaisini, J. R. Joseph, K. L. Lear, *IEEE J. Quantum Elect.* **2010**, *46*, 1590.

[220] K. Hiruma, M. Kinoshita, T. Mikawa, *IEEE T. Comp. Pack. Man.* **2011**, *1*, 420.

[221] K. D. Choquette, K. M. Geib, B. Roberds, H. Q. Hou, R. D. Twesten, B. E. Hammons, *Electron Lett.* **1998**, *34*, 1404.

[222] C. K. Lin, S. W. Ryu, P. D. Dapkus, *IEEE Phot. Technol. Lett.* **1999**, *11*, 1542.

[223] C. K. Lin, P. D. Dapkus, *IEEE Phot. Technol. Lett.* **2001**, *13*, 263.

[224] J. K. Tu, J. J. Talghader, M. A. Hadley, J. S. Smith, *Electron Lett.* **1995**, *31*, 1448.

[225] J. J. Talghader, *P. Soc. Photo-Opt. Ins.* **1998**, *3286*, 86.

[226] J. A. Lott, *Proc. SPIE* **2002**, *4649*, 203.

[227] J. A. Raley, J. A. Lott, T. R. Nelson, A. Stintz, K. J. Malloy, in *2002 Digest of the Leos Summer Topical Meetings* **2002**.

[228] K. Hiruma, M. Kinoshita, T. Mikawa, *J. Lightwave Technol.* **2005**, *23*, 4342.

[229] D. L. Mathine, R. Droopad, G. N. Maracas, *IEEE Phot. Technol. Lett.* **1997**, *9*, 869.

[230] D. Kang, S.-M. Lee, A. Kwong, J. Yoon, *Adv. Opt. Mater.* **2015**, DOI10.1002/adom.201400521.

[231] J. Chilla, Q. Z. Shu, H. L. Zhou, E. Weiss, M. Reed, L. Spinelli, *Proc. SPIE* **2007**, *6451*, 645109.

[232] L. W. Sang, M. Y. Liao, M. Sumiya, *Sensors-Basel* **2013**, *13*, 10482.

[233] C. Downs, T. E. Vandervelde, *Sensors-Basel* **2013**, *13*, 5054.

[234] J. H. Ahn, H. S. Kim, K. J. Lee, S. Jeon, S. J. Kang, Y. G. Sun, R. G. Nuzzo, J. A. Rogers, *Science* **2006**, *314*, 1754.

[235] H. C. Ko, M. P. Stoykovich, J. Z. Song, V. Malyarchuk, W. M. Choi, C. J. Yu, J. B. Geddes, J. L. Xiao, S. D. Wang, Y. G. Huang, J. A. Rogers, *Nature* **2008**, *454*, 748.

[236] H. C. Yuan, J. H. Shin, G. X. Qin, L. Sun, P. Bhattacharya, M. G. Lagally, G. K. Celler, Z. Q. Ma, *Appl. Phys. Lett.* **2009**, *94*, 013102.

[237] I. Jung, G. Shin, V. Malyarchuk, J. S. Ha, J. A. Rogers, *Appl. Phys. Lett.* **2010**, *96*, 021110.

[238] G. Shin, I. Jung, V. Malyarchuk, J. Z. Song, S. D. Wang, H. C. Ko, Y. G. Huang, J. S. Ha, J. A. Rogers, *Small* **2010**, *6*, 851.

[239] W. Q. Yang, H. J. Yang, G. X. Qin, Z. Q. Ma, J. Berggren, M. Hammar, R. Soref, W. D. Zhou, *Appl. Phys. Lett.* **2010**, *96*, 121107.

[240] I. W. Jung, J. L. Xiao, V. Malyarchuk, C. F. Lu, M. Li, Z. J. Liu, J. Yoon, Y. G. Huang, J. A. Rogers, *Proc. Natl. Acad. Sci. USA* **2011**, *108*, 1788.

[241] C. Namki, K. Munho, M. Zhenqiang, in *IEEE 10th Int. Conf. on Group IV Photonics (GFP)*, **2013**.

[242] Y. M. Song, Y. Z. Xie, V. Malyarchuk, J. L. Xiao, I. Jung, K. J. Choi, Z. J. Liu, H. Park, C. F. Lu, R. H. Kim, R. Li, K. B. Crozier, Y. G. Huang, J. A. Rogers, *Nature* **2013**, *497*, 95.

[243] C. C. Huang, X. D. Wu, H. W. Liu, B. Aldalali, J. A. Rogers, H. R. Jiang, *Small* **2014**, *10*, 3050.

[244] B. Corbett, L. Considine, S. Walsh, W. M. Kelly, *IEEE Phot. Technol. Lett.* **1993**, *5*, 1041.

[245] J. H. Seo, T. Y. Oh, J. Park, W. D. Zhou, B. K. Ju, Z. Q. Ma, *Adv. Funct. Mater.* **2013**, *23*, 3398.

[246] T. P. Grayson, *Proc. SPIE*, **2002**, *4849*, 269.

[247] S.-B. Rim, P. B. Catrysse, R. Dinyari, K. Huang, P. Peumans, *Opt. Express* **2008**, *16*, 4965.

[248] K. Itonaga, T. Arimura, K. Matsumoto, G. Kondo, K. Terahata, S. Makimoto, M. Baba, Y. Honda, S. Bori, T. Kai, K. Kasahara, M. Nagano, M. Kimura, Y. Kinoshita, E. Kishida, T. Baba, S. Baba, Y. Nomura, N. Tanabe, N. Kimizuka, Y. Matoba, T. Takachi, E. Takagi, T. Haruta, N. Ikebe, K. Matsuda, T. Niimi, T. Ezaki, T. Hirayama, in *2014 Symposium on VLSI Technology (VLSI-Technology)*, **2014**.